Universitat Autònoma de Barcelona

Multifunctional Materials based on TTF-PTM dyads: towards new Molecular Switches, Conductors and Rectifiers

Manuel Souto Salom

Tesi doctoral

Programa de Doctorat en Ciència de Materials

Directors

Prof. Jaume Veciana i Dr. Imma Ratera

Departament de Química

Facultat de Ciències

2016

Chapter 5

Nanostructuration of TTF-PTM dyads on surfaces

5.1. Introduction

One of the main challenges in molecular electronics is to understand and relate the chemical and electronic structure of an organic component to the performance of an electronic device.[1] Whereas properties of materials at macroscopic scale are well understood, new questions and challenges are faced at nanoscale where systems can show interesting physical behaviors based on quantum or subdomain phenomena. The development of new synthetic methods has allowed producing new uniform nanostructures with sizes ranging from 1 to 100 nm with distinct shapes and composition. One characteristic of these nanostructures is the presence of a high percentage of their constituent atoms at the surface exhibiting distinct physical properties since they have a different environment at the surface from those in bulk.[2]

5.1.1. Self-assembled monolayers (SAMs)

Self-assembled monolayers (SAMs) are a very well known methodology in order to functionalize surfaces based on the formation of organic assemblies by the adsorption of molecular constituents from solution or gas phase onto the surfaces of solids in a defined orientation and organized manner. Since the thickness of a SAM usually is in the order of 1-3 nm, it can be considered as the most elementary form of nanometer scale organic thin-film material.[2] Some of the advantages are the ease of preparation, versatility of the components and the modification of macroscopic properties by changing the structure at molecular level.

In general, the packing, orientation and physiochemical properties of the molecule on the surface are directly related with the three main parts of the SAM: a) a functional group, which will be used to tailor the desired properties of the surface; b) a molecular spacer, that will act over the molecular packing and depending on its nature could modify or not the electronic properties; and c) a linking group with a specific affinity for the substrate which will be responsible of the linkage between the organic compound and the surface (Figure 5.1). These different parts of the SAMs can be modified by chemical synthesis and will determine the physical properties of the surface. There are linking groups that depending on its nature can be specifically linked to different surfaces. However, most of the studied SAMs are based on alkanethiols grafted on gold due to the strong strength of the S-Au bond (~50 kcal/mol).

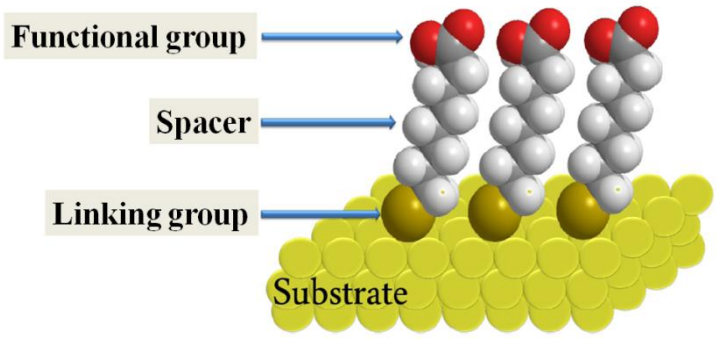

Figure 5.1. Schematic diagram of a SAM of alkanethiols on a gold surface with its principal parts.

The general procedure of SAM preparation consists on the immersion of a cleaned substrate into a solution of the functionalized organic molecules in some organic solvent during some hours at room temperature under inert atmosphere (Figure 5.2). The formation process can be described as follows. First, the molecules are adsorbed over the clean substrate in a disordered and fast manner. Then, a second step consists on the self-organization of the adsorbed molecules to form a well-defined structure with some lateral order. This reorganization process can take many hours in order to obtain the maximum density of molecules.

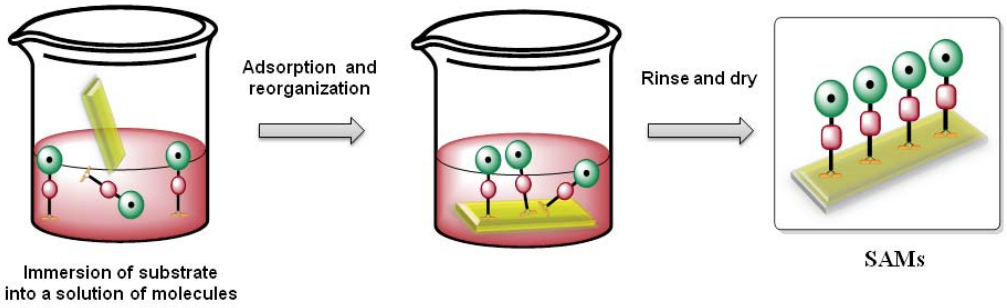

Figure 5.2. Schematic representation of the general steps for the preparation of SAMs.

There are some factors that can affect the final structure of the monolayer such as solvent, temperature, concentration, purity of the adsorbate, cleanness and flatness of the substrate.

a) Solvent: The effect of interactions of the solvent with the adsorbate and substrate can affect the kinetics of formation of monolayers and the mechanism of the assembly.
b) Concentration of adsorbate and immersion time: An optimal commitment between these two factors will give modified surfaces with high molecular coverage. These two parameters are inversely related since we normally need long immersion time for low adsorbate concentrations.
c) Purity of adsorbate: Presence of impurities on the molecules can influence the adsorption process and give place to important defects in the structure of the monolayers.
d) Cleanness, purity and flatness of the substrate: One of the most important issues is the use of a substrate with a high purity and flatness. In addition, the cleanness and activation of the substrate are important factors. In most of the cases, the method consists on washing the substrate with several solvents and a posterior UV/ozone surface cleaning method or acid treatment. A clean substrate, free of any dust, is required in order to avoid any foreign material previously adsorbed onto the substrate.

Once we know all the parameters that can affect the well formation and structure of the SAMs, we need to find the optimized conditions and experimental details in order to obtain reproducible and well organized molecular monolayers depending on each specific case.

5.1.2. Electrical conduction through SAMs

Understanding the electronic transport through a single molecule is of crucial importance for both fundamental and practical point of view in the field of molecular electronics. However, such process is very complicated and it will be necessary to take into account different contributions such as the mechanism of charge transfer from the electrodes to the molecules as well as the nature of molecule-electrode interactions. The study of charge transport through organic self-assembled molecular monolayers (SAMs) requires the preparation of a simple test device formed by a metal-molecular monolayer-metal junction.[3] Thus, this system is composed by two different metal-molecule interfaces. It is very important to investigate what is occurring at these interfaces in order to determine the final properties of the system. For doing so, it is necessary to consider the fabrication of stable molecular junctions, the characterization of their properties and the control of such properties.

Techniques employed for the fabrication of Metal/Molecule junctions

Different techniques have been developed in order to study the charge transport at the nanoscale since the metal/molecule interface will determine the stability and conductivity of single-molecule junctions. Such techniques are divided in two main groups: a) those which allow measuring electrical transport through a single molecule, and b) those techniques that measure the charge transport through a group of molecules organized as self-assembled monolayers (SAMs) using different kinds of top electrodes.

a) Charge transport through a single molecule

In single molecule measurements the molecule can be anchored to the electrodes through specific linking groups (-SH, -NH_2, -COOH) forming strong chemical bonds between the metal electrodes and the molecule conferring stability to the system.[4] This kind of molecular junction can be fabricated using Mechanically Controllable Break Junction (MCBJ) technique that consists on the trapping of molecules in a nanogap formed when a metal contact is broken in a solution of the functional molecules (Figure 5.3a).[3] Another possibility is to bind directly π-conjugated organic molecules to metallic electrodes in which the delocalized orbital hybridizes with the metal orbital (Figure 5.3b).[5]

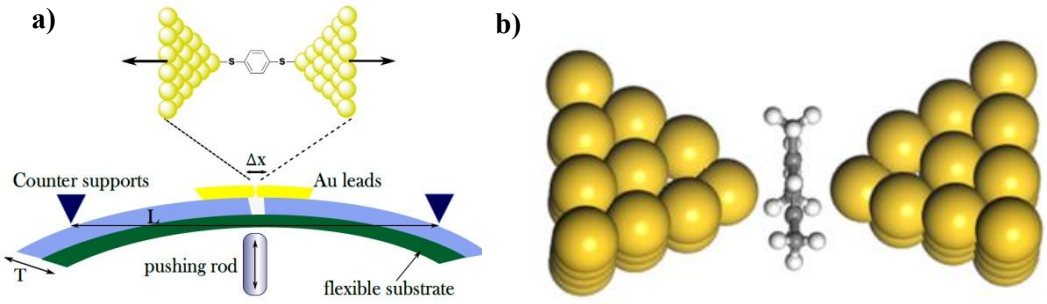

Figure 5.3. a) Scheme of single molecule junctions using the MCBJ technique and b) molecular junction formed directly with the electrodes.

b) Charge transport through SAMs

In order to measure the electron transport through a group of molecules (SAMs), there are different kinds of top electrodes to perform such measurements. For example, scanning-probe tips, Hg drops or an alloy of eutectic indium-gallium (EGain) are some of the top electrodes that have been widely used during the last years (Figure 5.4). These techniques present some limitations such as poor stability of the junctions, low reproducibility or low yields. For example, junctions using STM (or AFM) tips as top electrode exhibit a tunneling gap between the tip and the top of the SAM that could affect the charge transport measurements.[6] On the other hand, junctions using Hg as liquid-metal electrode contain a protective layer formed by short-alkyl chains that confers stability but also modify the resistivity of the system.[7]

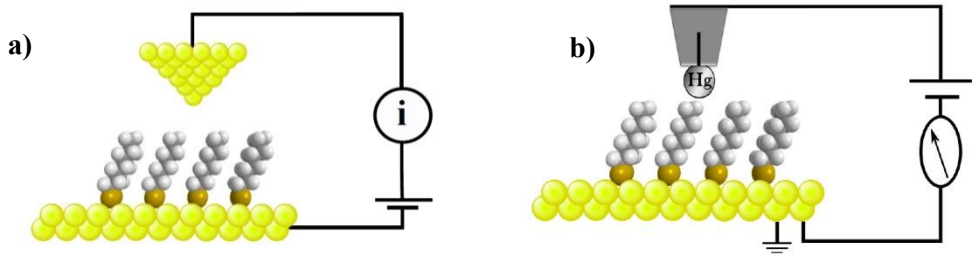

Figure 5.4. Schematic representation of molecular junctions using a) a scanning probe tip and b) a Hg drop as top electrode.

The junctions based on ultra-flat Au or Ag bottom electrodes (Au^{TS} or Ag^{TS}) and liquid metal (Ga_2O_3/EGaIn) top electrodes have been recently developed by Nijhuis, Whitesides *et al.* and show several advantages over other junctions (Figure 5.5).[8,9] The ultra-flat bottom electrode (Au^{TS} or Ag^{TS}) avoids failures from possible defects and the top electrode (Ga_2O_3/EGaIn) is less susceptible to short-circuiting the system than the mentioned Hg-drop obtaining higher yields of working functions. Moreover, this liquid electrode is nonvolatile, nontoxic and easy to handle. On the other hand, the layer of Ga_2O_3 shows a resistivity of several orders of magnitude less than the total resistance without any influence on the measurements.

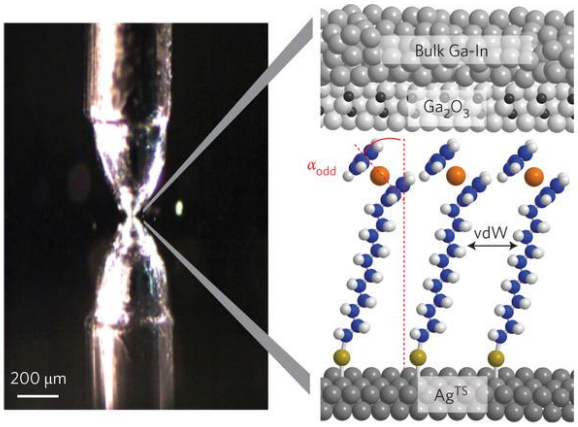

Figure 5.5. Schematic representation of the junctions of the type Ag^{TS} (bottom electrode) // SAM // Ga_2O_3/EGaIn (top electrode).

5.1.3. Self-assembled monolayers based on TTF derivatives

Preparation of SAMs of tetrathiafulvalene (TTF) derivatives on substrates has attracted a great deal of attention due to their interesting electrochemical properties and their potential application as molecular switches or ion sensors. These molecules exhibit three different redox states (i.e. neutral, radical cation and dication species) and thus can act as building blocks in switchable redox process since each state shows different physical properties such optical, magnetic or electrical properties.[10,11]

During the 80-90's several examples of Langmuir-Blodgett films of TTF derivatives were reported due to the high interest on their electrical conductive properties[12–17] and it was reported the immobilization of the carboxylic acid of TTF on RuO_2 and PtO_2 electrodes.[18] In 1994, Yip *et al.* reported for the first time the formation of stable TTF-functionalized SAMs on gold.[19] In 1998, Bryce and coworkers reported SAMs of TTF-crown derivatives that find application as electrochemically responsive detectors for metal cations (Figure 5.6a).[20] Then Fujihara reported a TTF compound containing four thiol groups forming very robust and stable SAMs on gold.[21] Echegoyen et *al.* also reported several crown-ether annelated TTFs forming stable SAMs on gold using multiple anchoring sites derived from thioctic acid that were employed to recognize alkali metal ions (Figure 5.6b).[22–25] Moreover, Pingarrón *et al.* studied the use of TTF derivatives SAMs for the construction of biosensors since they facilitate the electron transfer between the redox centre of an immobilized enzyme and the electrode substrate.[26]

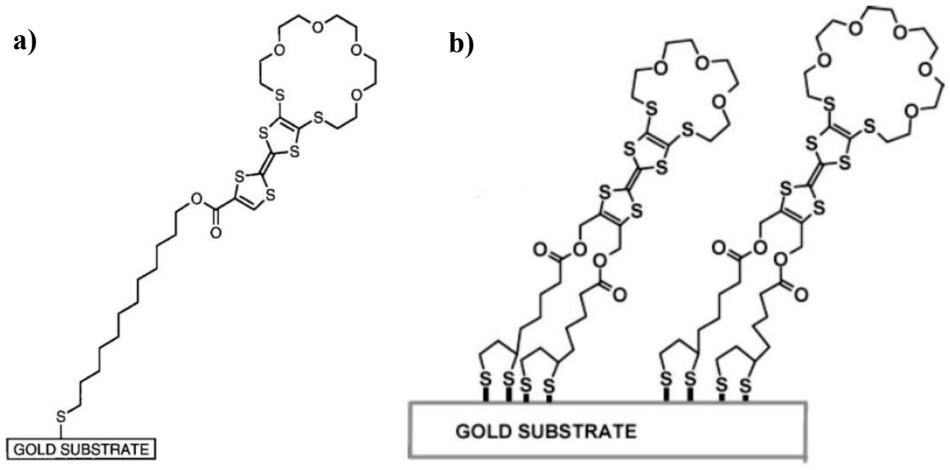

Figure 5.6. Schematic representation of SAMs formed by TTF-crown derivatives incorporating a) one[20] and b) four thiol anchoring groups.[25]

On the other hand, Lindsay *et al.* studied the conductivity of SAMs formed by TTF dithiolate derivatives on gold using c-AFM being proposed as candidate for molecular wires.[27] Other studies of TTF thiol derivatives SAMs on gold reported the relationship between the molecular packing arrangements (lateral interactions) in the SAMs and their electrochemical responses[28–30] as well as the electrochemical response when adding an electron-acceptor such as TCNQ on the surface.[31]

More recently, Sanguinet *et al.* reported the preparation of SAMs with TTF calyx[4]pyrroles functionalized with an acetyl-protected alkenethiol anchoring group and their potential use for chloride anion recognition (Figure 5.7a).[32] Moreover, Stoddart and coworkers have studied the use of TTF disulfide bared SAMs on gold for surface-enhancement Raman spectroscopy (SERS) applications (Figure 5.7b).[33]

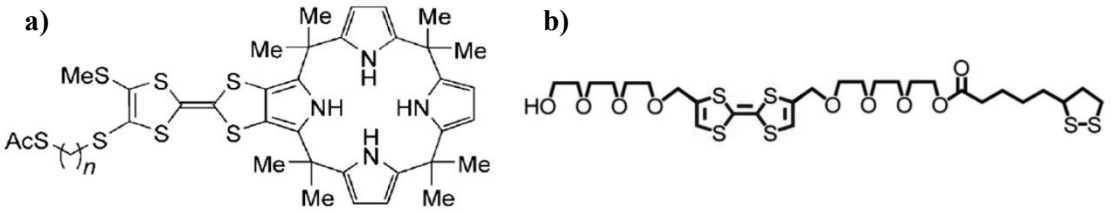

Figure 5.7. Molecular structure of a) mono-TTF calyx[4]pyrrole functionalized with an acetyl-protected alkenethiol and b) TTF disulfide derivative employed for SERS investigation.

Regarding the application as molecular switches, in the framework of our group it has been reported a SAM based on a TTF derivative on indium tin oxide (ITO) surface that operate as a ternary redox switch in which the magnetic and optical outputs are used as readout signals (Figure 5.8).[34,35] This molecular switch could find application for the development of ternary memory devices due to the robustness and stability of the system. Also it has been recently presented two disulfide TTF SAMs anchored on gold where the tuning of the surface wettability was achieved both electrochemically and chemically.[36]

Figure 5.8. Schematic representation of the electrochemical activity of TTF-triethoxysilane derivatives on ITO surface.

5.1.4. Self-assembled monolayers based on PTM radical derivatives

In the field of molecular electronics, the design and preparation of surfaces with tailored properties through functionalization with appropriated functional molecular building blocks is an important goal for the development of new memory devices and fabrication of high density data storage devices. In this sense, there is a high interest in the deposition of bistable molecules on surfaces that can be reversibly magnetically, optically or electrochemically interconverted between two different states exhibiting different output properties. One approach for this purpose is the preparation of SAMs of organic radicals since these systems can provide magnetic functionality to the surfaces.[37,38]

Functionalization of surfaces with polychlorotriphenylmethyl (PTM) radicals has been demonstrated to be a useful strategy in order to develop new molecular switches on surfaces. For example, in our group Crivillers *et al.* reported PTM SAMs on a SiO_2 surface that acted as a molecular switch between two stable states (the radical and the anion forms) combining electronic absorption, fluorescence emission and magnetic response as external outputs (Figure 5.9a).[39]

On the other hand, electroactive PTM derivatives were grafted on gold substrates using S-based binding groups and were fully characterized by electrochemistry showing high stability and large surface coverage (Figure 5.9b).[40] Moreover, conductivity measurements using conductive scanning force microscopy (C-SFM) through SAMs of the radical as well as on the closed-shell form of a PTM derivative on gold demonstrated that the radical SAMs were significantly more conductive.[41] Moreover, the charge transport characterization of the same SAMs revealed that both systems (closed- and open-shell forms of PTM) exhibit negative differential resistance (NDR) in their *I-V* curves which was attributed to similar resonant tunneling with unoccupied orbitals when large bias was applied.[42] A distinct PTM derivative functionalized with disulfide groups was also anchored to thick gold on a glass substrate and the SAMs were electrically commutable between the two stable redox states that exhibit different optical, magnetic and wetting properties.[43]

Finally, PTM derivatives functionalized with a silane group were anchored on indium tin oxide (ITO) which is a conducting and transparent substrate (Figure 5.9c). The SAMs were reversibly interconverted between the two states (radical and anion forms) upon application of an electrical input that was transduced into different optical and magnetic outputs. This molecular switch operated at very low voltages, can be patterned and addressed locally at the nanoscale, and showed a long term stability and reversibility.[44] In summary, SAMs of PTM radicals have demonstrated to be very promising systems for the development of non-volatile memory devices based on immobilized molecules.

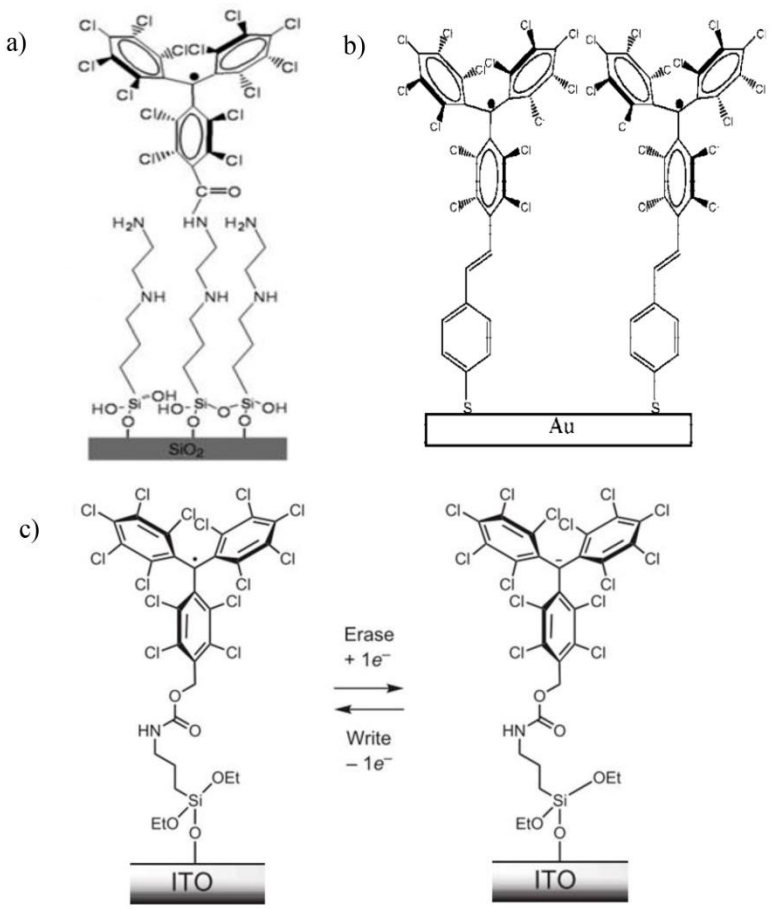

Figure 5.9. Schematic representation of a) SAMs of PTM radical derivatives on SiO_2, b) on Au, and c) electrochemical bistability of a SAM of PTM on ITO surfaces.

5.1.5. Donor-Acceptor dyads for molecular rectifying devices

In 1970, Aviram and Ratner theoretically proposed the first molecular rectifier that consisted on a donor-acceptor (D-A) molecule based on the electron-donor TTF unit linked to the electron-acceptor TCNQ linked through a non-conjugated bridge (TTF-σ-TCNQ) (Figure 5.10).[45] The reason of such behavior was ascribed to the asymmetrically distribution of electronic levels and the very low HOMO-LUMO gap (0.3 eV) that was imposed for the desired molecule. The purpose of the σ-bridge was to decouple the molecular orbitals of the donor moiety D from the molecular orbitals of the acceptor moiety A.

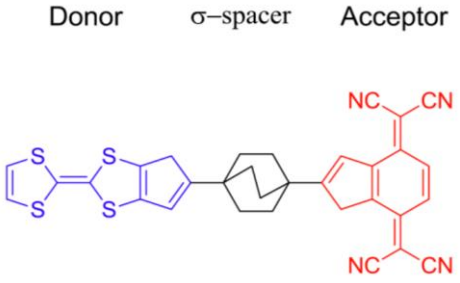

Figure 5.10. Molecular structure of the TTF-σ-TCNQ dyad proposed by Aviram and Ratner.[45]

The D-A rectification behavior in the Aviram-Ratner model can be understood from the energy diagram (Figure 5.11) which represents the arrangement of the molecular energy levels of the two subunits between two electrodes. When an external bias is applied (forward bias) an electron can travel from the Fermi level of the cathode to the empty LUMO of the acceptor and a similar process is produced in the other side of the junction where one electron is transferred from the HOMO of the donor to the anode. This electron process is irreversible as the LUMO level is higher in energy than the HOMO. On the other hand, if we apply a reverse bias to the same junction a much higher voltage is required to bring the Fermi level of the anode in resonance with the LUMO of the donor and the Fermi level of the anode in resonance with the HOMO of the acceptor.[46]

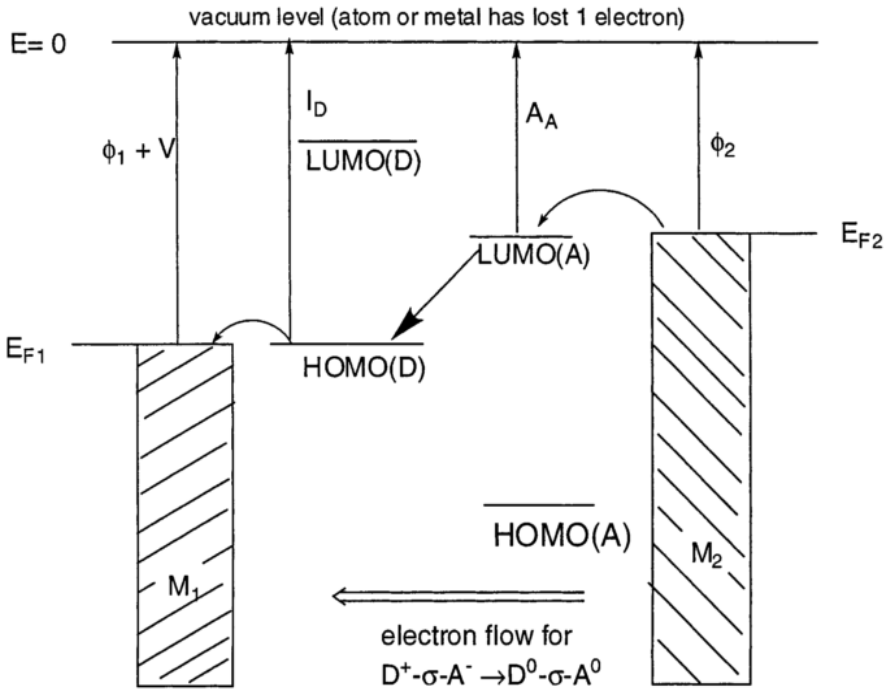

Figure 5.11. Electron flow from the excited zwitterion state D^+-σ-A^- to the undissociated ground-state D^0-σ-A^0 when the molecule is placed between two metal electrodes M_1 and M_2. Here, E = 0 is the vacuum level, ϕ is the work function of the metal electrodes, V is the potential applied on the left electrode (the right electrode is grounded), I_D is the ionization potential of the donor moiety D, A_A is the electron affinity of the acceptor moiety A, E_{F1} and E_{F2} are the Fermi levels of the metal electrodes, and the HOMO and LUMO levels are the highest occupied molecular orbitals or lowest unoccupied molecular orbitals of the D and A moieties.[46]

The original molecule proposed by Aviram and Ratner nor either molecule with similar HOMO-LUMO gap were never experimentally studied in molecular electronics due to the synthetic non availability of such molecules. However, since this first example suggested by Aviram and Ratner, several D-A systems have been investigated as candidates for molecular rectifiers including a) some D-σ-A with weak or moderate donor and acceptor moieties, b) conjugated D-π-A compounds and c) some molecules without an obvious asymmetry in the electronic structure.[1,46,47]

a) Molecular D-σ-A rectifiers

Aviram *et al.* reported in 1988 the first experimental study of rectification behavior of a D-σ-A dyad that was based on catechol (D) and quinone (A) moieties. The molecule was deposited as monolayer on gold and measured using a scanning tunneling microscopy (STM) tip as electrode.[48] Sambles *et al.* also reported the rectification behavior of a Langmuir-Blodgett (LB) film of a D-σ-A molecule based on TCNQ (A) and alkoxybenzene (D) derivatives (Figure 5.12a) that exhibited highly asymmetric *I-V* curves.[49] Mattern and coworkers studied a D-σ-A molecule based on a pyrene (D) and dinitrobenzene (A) (Figure 5.12b) as a LB multilayer. A five-layer of this molecule showed a rectification ratio of RR~130 at 2.5 V.[50] A family of PDI-based molecular rectifiers were studied by Metzer and coworkers as LB monolayers between two gold electrodes.[51] For example, Fc-σ-PDI dyad (Figure 5.12c) showed rectification ratio of ~14-28 at ±1 V which showed HOMO and LUMO energy levels closed to the work function of the electrodes. The first TTF-σ-A molecular rectifier was reported by Bryce et *al.*, based on a TTF-σ-fluorene dyad, where rectification behavior increased upon alignment of the molecules in LB monolayers (Figure 5.12d).[52]

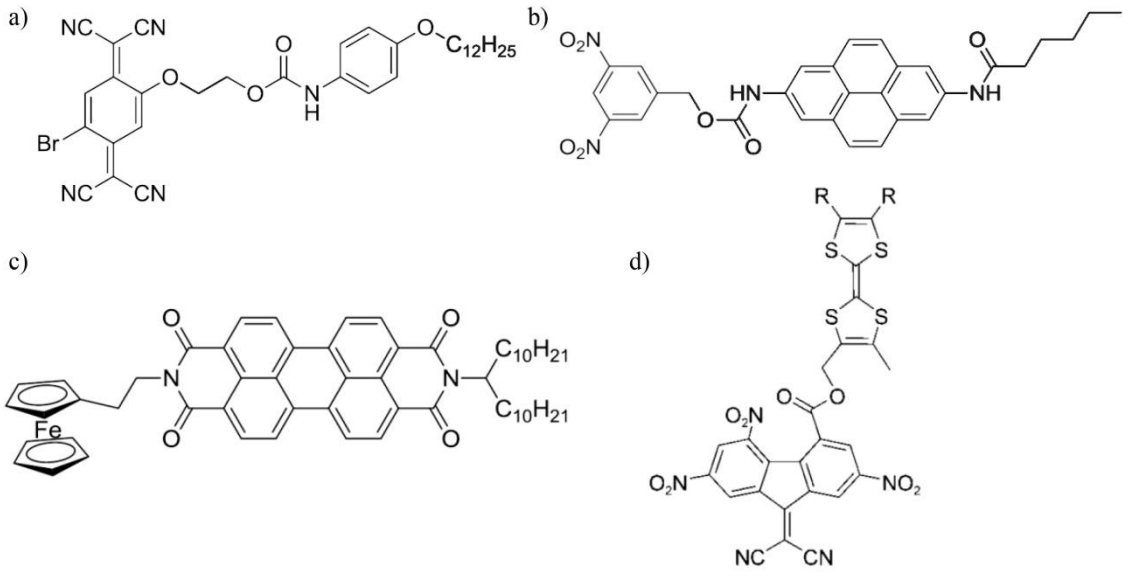

Figure 5.12. Molecular structures of different D-σ-A dyads proposed as molecular rectifiers: a) TCNQ-σ-alkoxybenzene, b) dinitrobenzene-σ-pyrene, c) Fc-σ-PDI, and d) TTF-σ-fluorene dyads.

b) Molecular D-π-A rectifiers

Regarding the D-π-A dyads, Metzger *et al.* reported an exhaustive study of the electrical rectification in hexadecylquinolinium-tricyanoquinodimethanide dyad (Figure 5.13a) where the twist angle, caused by steric hindrance between the donor and acceptor moieties, provided a good separation of HOMO and LUMO orbitals and, thus, showed rectification behavior.[53,54] In a similar approach, Ashwell and coworkers reported a comparison between the rectification behavior of several SAMs of quinolinium hemicyanine dye derivatives on gold exhibiting asymmetric *I-V* characteristics.[55] Interestingly, SAMs with sterically hindered D-π-A moieties, in which the donor and acceptor were twisted out of plane, exhibited rectification, whereas those that are planar did not. A similar behavior was observed for two rectifying dyes with an heterocyclic donor and $C(CN)_2$ as acceptor (Au-S-C_nH_{2n}-P3CNQ) where one of the dyads has a methyl substituent that produces a significant twist angle between the donor and acceptor (Figure 5.13b). Thus, the higher conjugation in the planar molecule (Figure 13c) leads to a higher delocalization of HOMO and LUMO throughout the entire molecule that has a detrimental influence for the rectification behavior.[56]

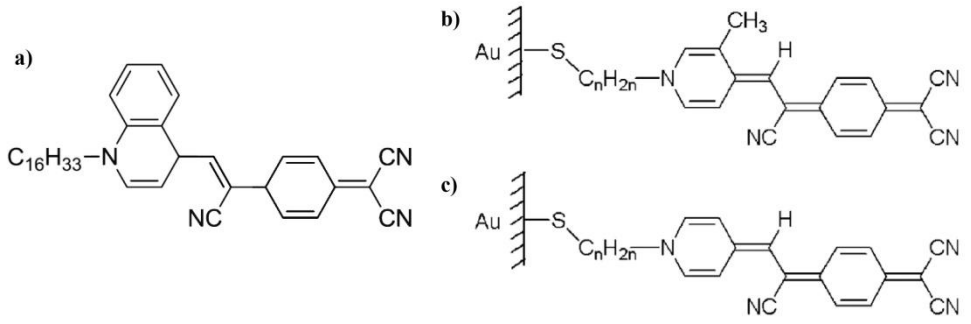

Figure 5.13. Molecular structures of a) mexadecylquinolinium-π-tricyanoquinodimethanide dyad, b) Au-S-C_nH_{2n}-(Me)P3CNQ and c) C_nH_{2n}-P3CNQ.

More recently, Perepichka *et al.* have developed some donor-acceptor dyads (NDI-EDOT) functionalized with a thiol group that allow covalent attachment to gold electrodes (Figure 5.14). The bridge consisted on a phenyl group to separate the donor and acceptor moieties giving an efficient separation between the HOMO and LUMO orbitals.[57]

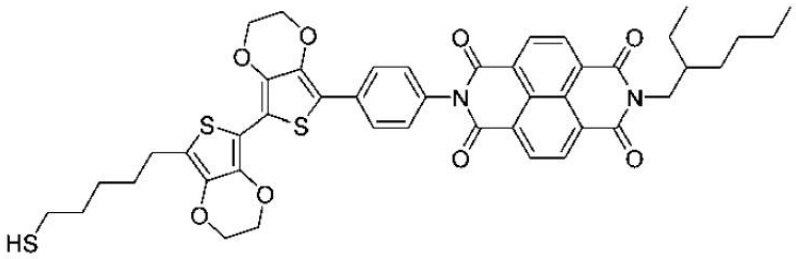

Figure 5.14. Molecular structure of the NDI-EDOT-SH dyad.

c) Asymmetric molecular rectifiers

Yu and coworkers reported diode molecules based on thiophene-thiazole diblock polymers with terminal thiol groups in order to assemble the diode with controlled orientations between two gold electrodes (Figure 5.15). By manipulating the orientation of the diode molecules it was possible to control the rectification directions indicating that the dipole moments play an important role in determining the rectifying direction and ratio.[58]

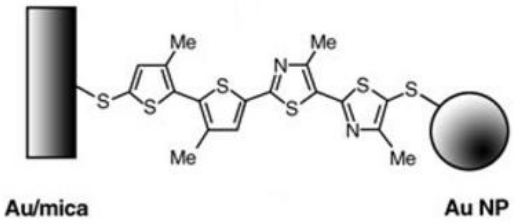

Figure 5.15. Schematic representation of a thiophene-thiazole diblock polymer between two terminal gold electrodes.

In a similar approach, current rectification was observed for other non-symmetric diblock dipyrimidinyl-diphenyl molecule covalently bound to two gold electrodes whereas a symmetric tetraphenyl block displays a perfect symmetric behavior (Figure 5.16). An important issue of these studies were the knowledge of the orientation of the molecules within the junction that can be controlled by a selective deprotection of each thiol terminal group.[59]

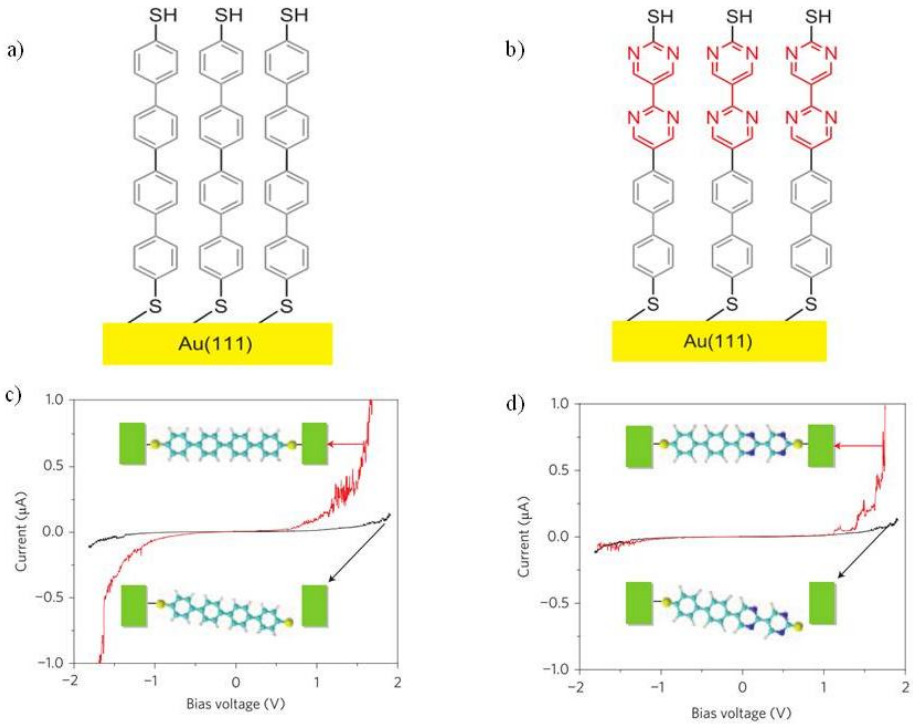

Figure 5.16. a) Symmetric tetraphenyl molecules and b) non-symmetric dipyridiminyl-diphenyl molecule. I-V curves for the c) symmetric tetratphenyl and d) asymmetric dipyridiminyl-diphenyl molecules.

During these last years, some other rectifying junctions with no D-bridge-A structures have been reported that are not based on the Aviram-Ratner model (two conductive molecular orbitals) but on one conductive molecular orbital.[46,47] The groups of Williams and Baranger proposed that molecular tunneling junctions with a single conductive molecular orbital placed close to the Fermi levels of the electrodes and asymmetrically coupled to one of the electrodes can rectify.[60,61] These molecules consists of three main parts (Fig 5.17a): a) an anchoring group to attach the molecules to electrodes, b) a conductive part with an accessible HOMO or LUMO orbital and c) insulating groups of different lengths to provide asymmetry.[9] For example, the cobaltocene (Figure 5.17b) was proposed as a molecular rectifier as it contains a conductive HOMO level centered at the Co, is energetically positioned above the Fermi levels and asymmetrically coupled to each electrode.

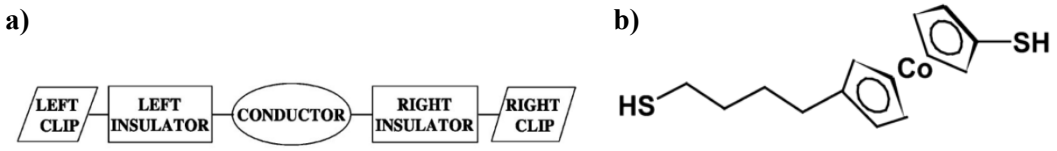

Figure 5.17. a) Schematic structure of an asymmetric tunneling barrier molecular rectifier. b) Molecular structure of the cobaltocene derivative.

In a similar approach, Nijhuis and Whitesides reported an exhaustive study of the conductivity of junctions with ultra-flat Ag bottom electrodes and liquid metal (EGaIn) top electrode, based on SAMs of alkanethiolates with conductive ferrocene (Fc) head groups modifying the proximity of the redox centre to each electrode.[9,8,62] Interestingly, it was observed that junctions with the Fc unit placed symmetrically between the two electrodes didn't rectify whereas when the Fc moiety was placed closer to one electrode junctions showed rectification behavior (Figure 5.18).

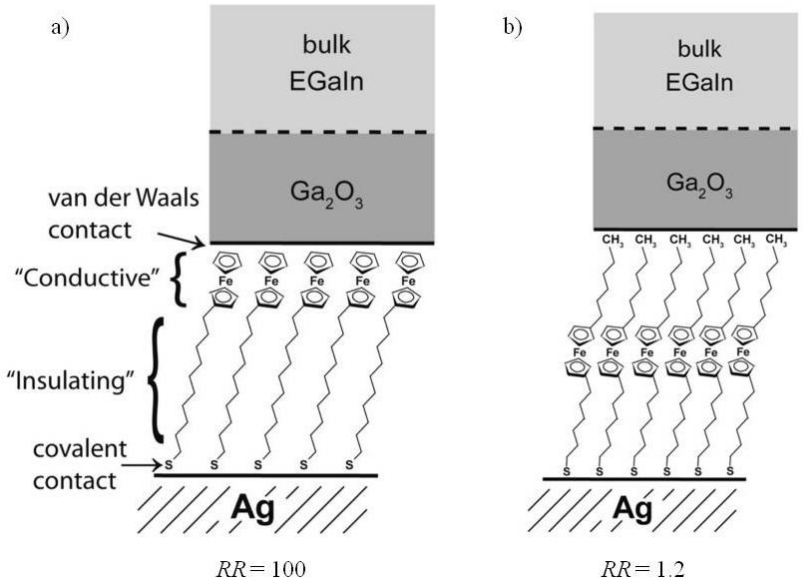

Figure 5.18. Idealized schematic representations of the tunneling junctions consisting of Ag bottom electrodes, SAMs of Fc-alkanethiolates derivatives and Ga_2O_3/EGaIn top electrodes. *RR* is the rectification ratio for junctions with SAMs as R = |J(V)|/|J(-V)|.

5.1.6. Fc-PTM dyads as molecular rectifiers

In view of the potential application of D-A systems as molecular rectifiers and the interesting properties of the organic radicals anchored into surfaces, in our group we have synthesized two D-A dyads based on a ferrocene (Fc) moiety as electron donor linked to a PTM electron acceptor unit, either in their non-radical (DT-Fc-PTM-NR) and in the radical form (DT-Fc-PTM-R), functionalized with a cyclic disulfide group (Figure 5.19). In collaboration with the group of Prof. Nijhuis, we have studied the ability to transport charge of SAMs formed by these two dyads as well as by the Fc-disulfide derivative (DT-Fc). Ultraflat template-stripped Au surfaces (Au^{TS}) supported these SAMs and an eutectic alloy of gallium and indium (EGaIn), covered with a skin of gallium oxide formed electrical contacts with them. Moreover, we fully characterized the SAMs by cyclic voltammetry (CV), X-ray photoemission spectroscopy (PES) and Near-edge X-ray absorption (NEXAFS) in order to study the electronic structures of the molecules anchored on gold surface.[64]

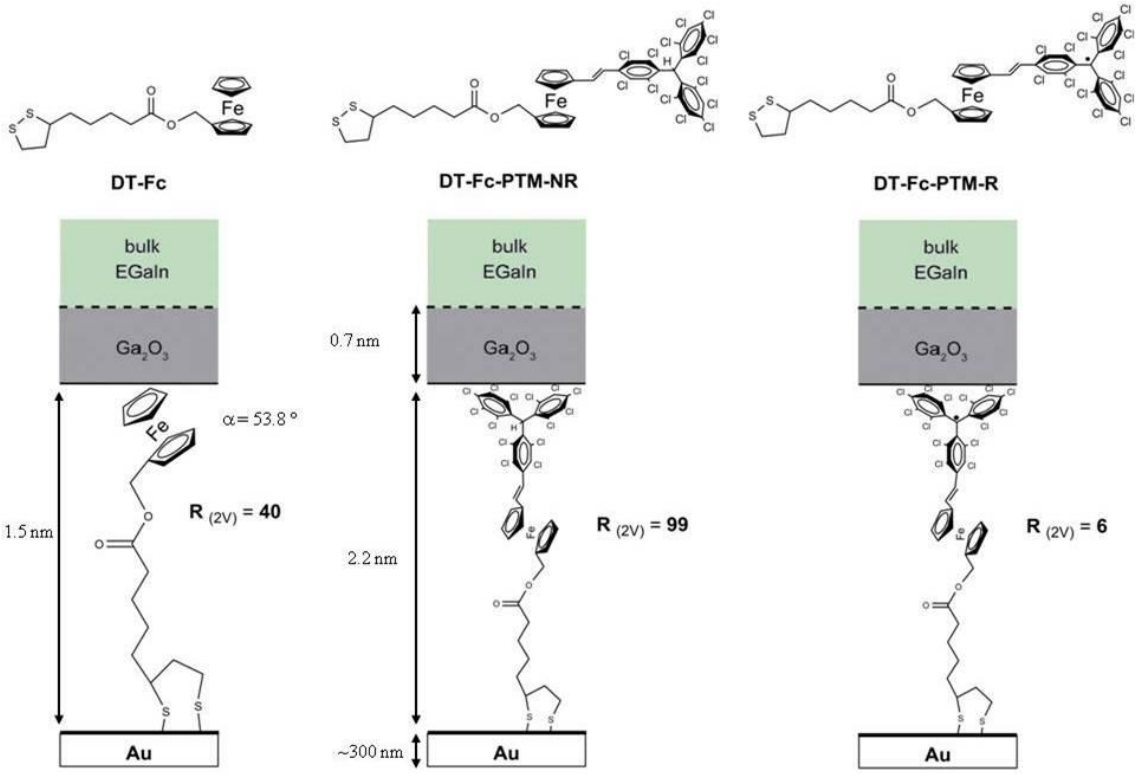

Figure 5.19. Molecular structures of **DT-Fc**, **DT-Fc-PTM-NR** and **DT-Fc-PTM-R**, and idealized schematic representations of the junctions consisting on Au bottom electrodes, the corresponding SAMs and Ga_2O_3/EGaIn top electrodes. *R* is the rectification ratio for junctions with SAMs as R = |J(V)|/|J(-V)|.

Interestingly, the non-radical PTM derivative shows a rectification ratio of *c.a.* 10^2 which was two orders of magnitude larger than its radical analogous. This different rectifying behavior could be attributed to the higher HOMO-LUMO delocalization in the radical derivative, characterized by the presence of the IET band in the UV-vis-NIR spectrum, due to the enhanced electron-acceptor character of the PTM radical moiety that produces a higher intramolecular interaction between the donor and acceptor units.

5.2. Results and discussion

In order to understand better the origin of rectification ratio occurring in junctions made with D-A molecules where the acceptor moiety is a PTM radical we decided to prepare a junction of such type but with a TTF moiety as a donor instead of a ferrocene (Fc). The obtaining results and discussion of the charge transport properties is reported in this Section.

5.2.1. Self-assembled monolayers based on TTF-PTM dyads

For such purpose, we designed and synthesized two new D-A dyads based on a TTF unit linked through a vinylene π-bridge to a PTM radical in its radical (**6**) and non-radical form (**6-H**) that were functionalized with a disulfide group to form SAMs on gold surfaces (Figure 5.20). These SAMs were also fully characterized by different techniques such as cyclic voltammetry, ToF-SIMs, ESR, XPS and NEXAFS in order to analyze the electronic properties and stability of the SAMs. Moreover, also in collaboration with the group of Prof. Nijhuis (National Unversity of Singapore), EGaIn junctions were used to study and discuss the electron transport through SAMs of **6** and **6-H** that exhibited different rectification behavior (see Publication #6).

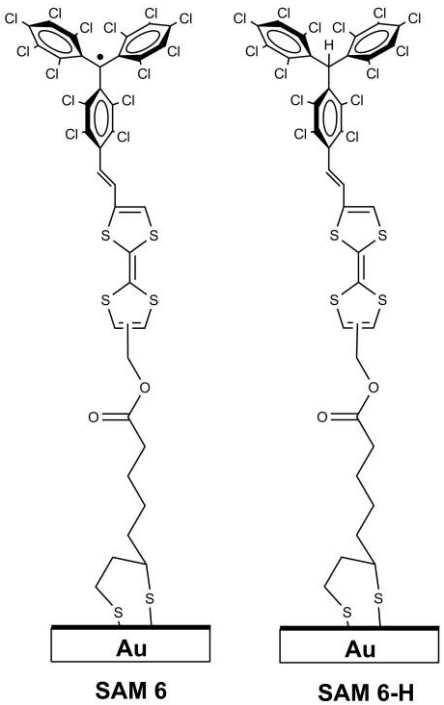

Figure 5.20. Idealized schematic representation of self-assembled monolayers formed by **6** (**SAM 6**) and **6-H** (**SAM 6-H**) on gold.

Cyclic voltammetries of the SAMs gave us information about the possible redox states for each dyad (Figure 5.21). In **SAM 6** we observed three different peaks that are assigned to the reduction of the PTM radical unit and to the oxidation of the TTF moiety to $TTF^{+\cdot}$ and TTF^{2+}, respectively. On the other hand, CV of **SAM 6-H** showed only two reversible redox peaks as the non-radical PTM moiety is not an electroactive species anymore.

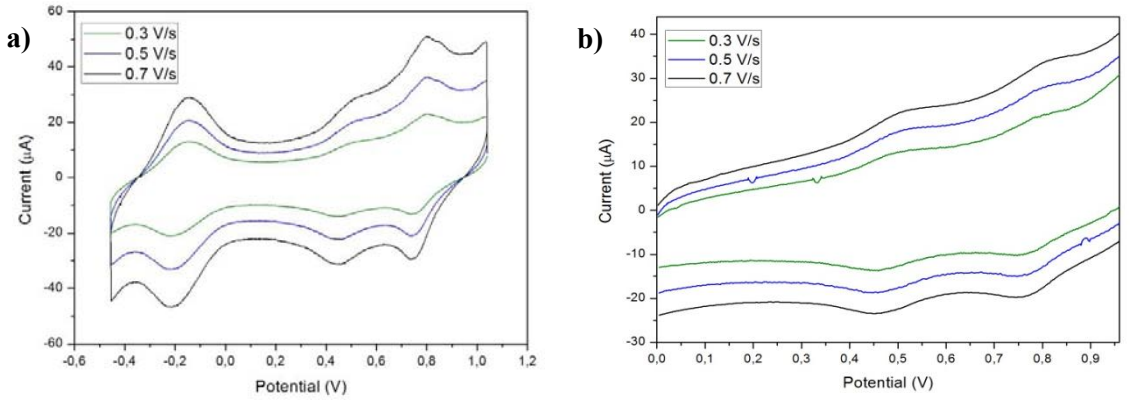

Figure 5.21. Cyclic voltammetries of a) **SAM 6** and b) **SAM 6-H** on Au as working electrode, Pt as counter electrode, and Ag/AgCl as reference electrode, recorded at different scan rates with 0.1M $LiClO_4$ solution in acetonitrile as electrolyte.

On the other hand, photoemission and Near-Edge X-ray Absorption (NEXAFS) measurements, performed at Elettra synchrotron, gave us information about the electronic structure of the SAMs. More specifically, from the valence band we could estimate the HOMO energy values located on the TTF moieties that were in agreement with the electrochemical data. On the other hand, NEXAFS measurements gave us information about the unoccupied orbitals of the two nanostructured dyads (Figure 5.22). The main difference between the spectra of the radical and non radical SAM was the appearance of a small peak at 282.6 eV observed in the open-shell monolayer (**SAM 6**) that was absent in the closed-shell protonated monolayer (**SAM 6-H**). This peak was assigned to the single unoccupied molecular orbital (SUMO) of the PTM radical units.[63]

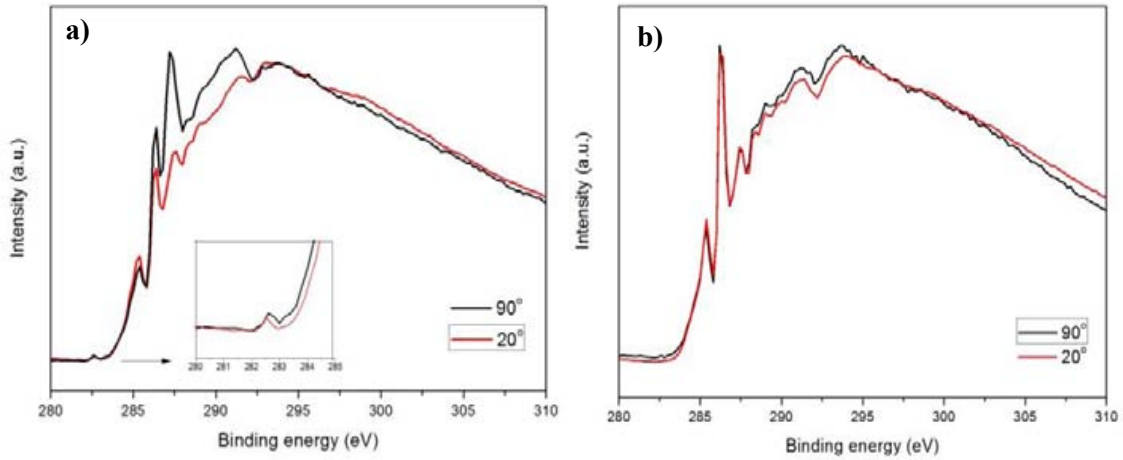

Figure 5.22. NEXAFS spectra of a) **SAM 6** and b) **SAM 6-H** in normal (NI, red line, 90º) and grazing (GI, black line, 20º) incidences. Input shows the zoom in the 280-285 eV region.

Finally, stable and reproducible molecular junctions based on **SAMs 6** and **6-H** were prepared on template-stripped gold (Au^{TS}) surface, used as a bottom electrode, and eutectic indium-gallium (EGaIn) metallic alloy, with a surface layer of Ga_2O_3, as the top contact. Charge transport measurements through SAMs were measured with a bias voltage ranged from +2.0 to -2.0 V (Figure 5.23). The most remarkable difference between the charge transport measurements for the two systems was the rectification properties. Thus, the junctions formed by **SAM 6** didn't show any rectification behavior whereas measurements on the junctions formed by **SAM 6-H** showed a moderate rectification ratio of RR = ~13 at |V|=2.0 V. The difference between both systems could be due to the higher HOMO delocalization of the TTF moiety through the PTM radical in **6** in comparison with **6-H** as it was previously observed for the DT-Fc-PTM dyads. This overlap between the donor and acceptor units in radical dyad **6** is in agreement with the intramolecular charge transfer (ICT) band observed in the absorption spectrum of the radical dyad. It is important to note that the rectification ratios for both SAMs **6** and **6-H** are much lower (RR~13) than the values obtained for the DT-Fc-PTM-NR dyad (~100) indicating that the donor unit could play an important role in the rectification mechanism for this kind of donor-acceptor systems.

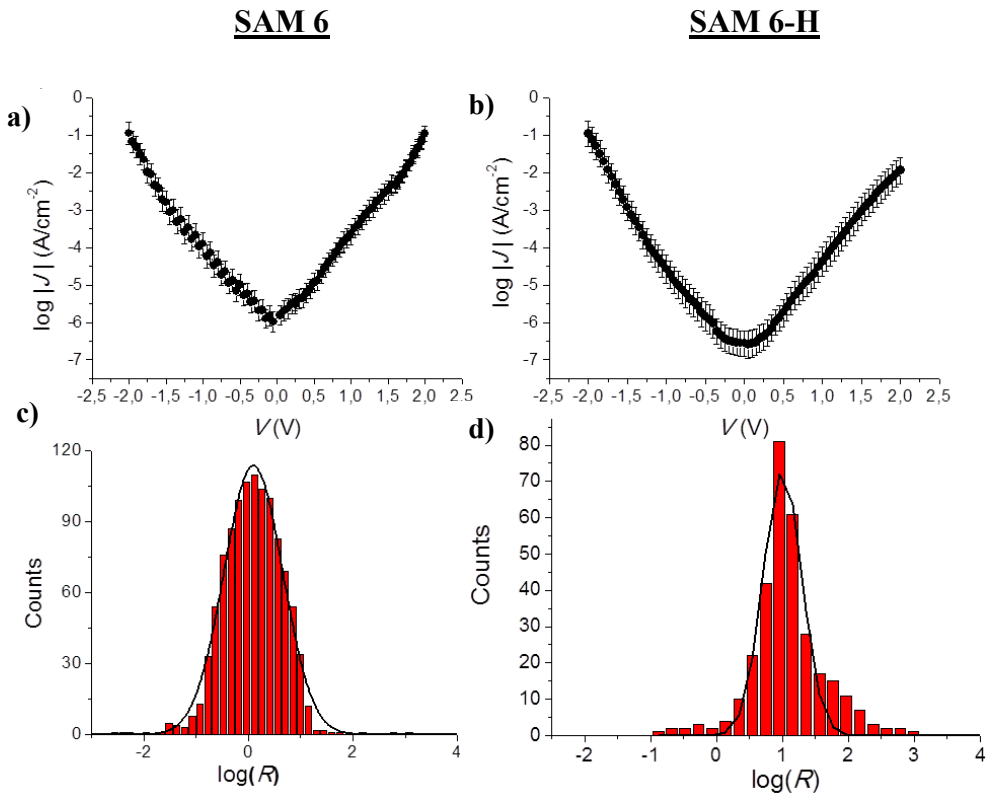

Figure 5.23. *Top*: Absolute current densities, J (A/cm^2), plotted vs voltages (*V*) of the junctions a) **Au_{TS}-SAM6//Ga_2O_3/EGaIn**, b) **Au_{TS}-SAM6-H//Ga_2O_3/EGaIn**. *Bottom*: Histogram with a Gaussian fit of the rectification ratio, RR at $|V| = 2.0$ V, of the junctions for c) **SAM 6** and d) **SAM 6-H**.

5.3. Summary

In summary, in this Chapter we have reported the synthesis and characterization of a new TTF-PTM radical dyad functionalized with a disulfide group in order to form self-assembled monolayers on gold surfaces. Moreover, its non-radical analogue dyad, which has a similar molecular structure but different electronic structure, was also obtained to study the influence of electronic structure on the charge transport mechanism. An exhaustive characterization of both SAMs was performed by cyclic voltammetry, ToF-SIMs, XPS and NEXAFS. CV experiments demonstrating the stability of the SAMs and NEXAFS spectra revealed the appearance of the SUMO band attributed to the radical dyad (**Publication #6**).

Finally, stable and reproducible EGaIn junctions with SAMs of radical dyad **6** didn't show any rectification behavior whereas junctions with SAMs of non-radical dyad **6-H** showed a moderate rectification ratio of ~13 at |V| = 2.0 V. This difference could be attributed to a higher delocalization of the HOMO orbital of TTF through the PTM radical in the radical dyad **6** than in the non-radical **6-H**. We believe that a improvement of the localization of the HOMO orbital of TTF achieved by either the incorporation of a σ-bridge between the donor and acceptor units or by twisting both units could provide an efficient separation of the HOMO and LUMO orbitals and thus to an enhancement of the rectification ratio of the SAMs. In conclusion, these D-A radical systems anchored in surfaces have been proposed as promising molecular building blocks for the development of new molecular switches and rectifiers.

5.4. References

1. Metzger, R. M. Unimolecular Electronics. *Chem. Rev.* **115,** 5056–5115 (2015).

2. Love, J. L., Estroff, L. A., Kriebel, J. K., Nuzzo, R. G. & Whitesides, G. M. Self-Assembled Monolayers of Thiolates on Methals as a Form of Nanotechnology. *Chem. Rev.* **105,** 1103–1169 (2005).

3. Reed, M. A., Zhou, C., Muller, C. J., Burgin, T. P. & Tour, J. M. Conductance of a Molecular Junction. *Science* **278,** 252–254 (1997).

4. Chen, F., Li, X., Hihath, J., Huang, Z. & Tao, N. Effect of Anchoring Groups on Single-Molecule Conductance : Comparative Study of Thiol-, Amine-, and Carboxylic-Acid-Terminated Molecules. *J. Am. Chem. Soc.* **128,** 15874–15881 (2006).

5. Kiguchi, M. *et al.* Highly conductive molecular junctions based on direct binding of benzene to platinum electrodes. *Phys. Rev. Lett.* **101,** 04681 (2008).

6. Engelkes, V. B., Beebe, J. M. & Frisbie, C. D. Analysis of the Causes of Variance in Resistance Measurements on Metal - Molecule - Metal Junctions Formed by Conducting-Probe Atomic Force Microscopy. *J. Phys. Chem. B* **109,** 16801–16810 (2005).

7. Haag, R., Rampi, M. A., Holmlin, R. E. & Whitesides, G. M. Electrical Breakdown of Aliphatic and Aromatic Self-Assembled Monolayers Used as Nanometer-Thick Organic Dielectrics. *J. Am. Chem. Soc.* **121,** 7895–7906 (1999).

8. Nijhuis, C. A., Reus, W. F. & Whitesides, G. M. Molecular rectification in metal-SAM-metal oxide-metal junctions. *J. Am. Chem. Soc.* **131,** 17814–17827 (2009).

9. Nijhuis, C. A., Reus, W. F. & Whitesides, G. M. Mechanism of rectification in tunneling junctions based on molecules with asymmetric potential drops. *J. Am. Chem. Soc.* **132,** 18386–18401 (2010).

10. Canevet, D., Sallé, M., Zhang, G., Zhang, D. & Zhu, D. Tetrathiafulvalene (TTF) derivatives: key building-blocks for switchable processes. *Chem. Commun.* **7345,** 2245–2269 (2009).

11. Gomar-nadal, E., Puigmartı, J. & Amabilino, D. B. Assembly of functional molecular nanostructures on surfaces. *Chem. Soc. Rev.* **37,** 490–504 (2008).

12. Dhindsa, A. S., Bryce, M. R., Lloyd, J. P. & Petty, M. C. A highly conducting tetrathiafulvalene Langmuir-Blodgett film. *Thin Solid Films* **165,** 97–100 (1988).

13. Dhindsa, A. S., Bryce, M. R., Lloyd, J. P. & Petty, M. C. Electroactive Langmuir-Blodgett films of Hexadecanoyl-TTF. *Synth. Met.* **27,** 563–568 (1988).

14. Pearson, C., Dhindsa, A. S., Bryce, M. R. & Petty, M. C. Alternate-layer Langmuir-Blodgett Films of Long-chain TCNQ and TTF derivatives. *Synth. Met.* **31,** 275–279 (1989).

15. Naito, K., Miura, A. & Azuma, M. Langmuir-Blodgett Film Assembly of Novel Dye Molecules Substituted by a Steroid Skeleton: Molecular Design for Uniform Films. *J. Am. Chem. Soc.* **113,** 6386–6395 (1991).

16. Search, H., Journals, C., Contact, A., Iopscience, M. & Address, I. P. An electrical investigation into multilayer assemblies of charge-transfer materials. *J. Phys. D* **1422,** 1422–1429 (1991).

17. Goldenberg, L. M. *et al.* Langmuir – Blodgett films of a tetrathiafulvalene derivative substituted with an azobenzene group. *J. Mater. Chem.* **7,** 20133–20137 (1997).

18. Kuo, K., Moses, P. R., Lenhard, J. R., Green, D. C. & Murray, R. W. Immobilization , Electrochemistry , and Surface Interactions of Tetrathiafulvalene on Chemically Modified Ruthenium and Platinum Oxide Electrodes. *Anal. Chem.* **51,** 745–748 (1979).

19. Yip, C. M. & Michael, D. Self-Assembled Monolayers with Charge-Transfer Groups : n-Mercaptoalkyl Tetrathiafulvalenecar boxylate on Gold. *Langmuir* **10,** 549–556 (1994).

20. Moore, A. J. *et al.* Cation recognition by self-assembled layers of novel crown-annelated tetrathiafulvalenes. *Adv. Mater.* **10,** 395–398 (1998).

21. Fujihara, H., Nakai, H., Yoshihara, M. & Maeshima, T. Alkane-tetrathiol induced formation of remarkably stable self-assembled monolayer and polymer films containing electroactive tetrathiafulvalene moieties on metal electrodes. *Chem. Commun.* 737–738 (1999).

22. Liu, H., Liu, S. & Echegoyen, L. Remarkably stable self-assembled monolayers of new crown-ether annelated tetrathiafulvalene derivatives and their cation recognition properties. *Chem. Commun.* **100,** 1493–1494 (1999).

23. Liu, S. G., Liu, H., Bandyopadhyay, K., Gao, Z. & Echegoyen, L. Dithia-crown-annelated tetrathiafulvalene disulfides: Synthesis, electrochemistry, self-assembled films, and metal ion recognition. *J. Org. Chem.* **65,** 3292–3298 (2000).

24. Tripp, G. *et al.* Self-assembled monolayers of a tetrathiafulvalene-based redox-switchable ligand. *New J. Chem.* **26,** 1320–1323 (2002).

25. Herranz, M. A., Yu, L., Martín, N. & Echegoyen, L. Synthesis, Electrochemistry and Self-Assembled Monolayers of Novel Tetrathiafulvalene (TTF) and π-Extended TTF (exTTF) Disulfides. *J. Org. Chem.* **68,** 8379–8385 (2003).

26. Campuzano, S., Pedrero, M., Montemayor, C., Fatás, E. & Pingarrón, J. M. Tetrathiafulvalene thiolated derivatives self-assembled monolayers as platforms for the construction of electrochemical biosensors. *Electrochem. commun.* **8,** 299–304 (2006).

27. Gomar-Nadal, E. *et al.* Self-assembled monolayers of tetrathiafulvalene derivatives on Au(111): Organization and electrical properties. *J. Phys. Chem. B* **108,** 7213–7218 (2004).

28. Yokota, Y. *et al.* Dynamic and collective electrochemical responses of tetrathiafulvalene derivative self-assembled monolayers. *J. Phys. Chem. B* **110,** 20401–20408 (2006).

29. Hsu, S., Reinhoudt, D. N. & Velders, A. H. Lateral interactions at functional monolayers. *J. Mater. Chem.* **21,** 2428–2444 (2011).

30. Gautier, C. *et al.* Intermolecular interactions in self-assembled monolayers of tetrathiafulvalene derivatives. *Phys. Chem. Chem. Phys.* **13,** 2118–2120 (2011).

31. Pacsial, E. J., Alexander, D., Alvarado, R. J., Tomasulo, M. & Raymo, F. M. Donor / Acceptor Interactions in Self-Assembled Monolayers and Their Consequences on Interfacial Electron Transfer. *J Phys Chem B* **108,** 19307–19313 (2004).

32. Jensen, L. G. *et al.* Self-Assembled Monolayers of Mono-Tetrathiafulvalene Calix[4]pyrroles and Their Electrochemical Sensing of Chloride. *Chem. Eur. J.* **15,** 8128–8133 (2009).

33. Paxton, W. F., Kleinman, S. L., Basuray, A. N., Stoddart, J. F. & Van Duyne, R. P. Surface-enhanced Raman spectroelectrochemistry of TTF-modified self-assembled monolayers. *J. Phys. Chem. Lett.* **2,** 1145–1149 (2011).

34. Simão, C. *et al.* A three-state surface-confined molecular switch with multiple channel outputs. *J. Am. Chem. Soc.* **133,** 13256–13259 (2011).

35. Simao, C. *et al.* Intramolecular electron transfer in the photodimerisation product of a tetrathiafulvalene derivative in solution and on a surface. *Chem. Sci.* **4,** 307 (2013).

36. Casado-Montenegro, J. *et al.* Electrochemical and chemical tuning of the surface wettability of tetrathiafulvalene self-assembled monolayers. *Chem. Commun.* **49,** 8084–6 (2013).

37. Mas-Torrent, M. *et al.* Organic radicals on surfaces: towards molecular spintronics. *J. Mater. Chem.* **19,** 1691–1695 (2009).

38. Mas-Torrent, M., Crivillers, N., Rovira, C. & Veciana, J. Attaching persistent organic free radicals to surfaces: How and why. *Chem. Rev.* **112,** 2506–2527 (2012).

39. Crivillers, N. *et al.* Self-assembled monolayers of a multifunctional organic radical. *Angew. Chemie - Int. Ed.* **46,** 2215–2219 (2007).

40. Crivillers, N., Mas-Torrent, M., Vidal-Gancedo, J., Veciana, J. & Rovira, C. Self-assembled monolayers of electroactive polychlorotriphenylmethyl radicals on Au(111). *J. Am. Chem. Soc.* **130,** 5499–5506 (2008).

41. Crivillers, N. *et al.* Dramatic influence of the electronic structure on the conductivity through open- and closed-shell molecules. *Adv. Mater.* **21,** 1177–1181 (2009).

42. Crivillers, N. *et al.* Negative differential resistance (NDR) in similar molecules with distinct redox behaviour. *Chem. Commun.* **47,** 4664–4666 (2011).

43. Simão, C., Mas-torrent, M., Veciana, J. & Rovira, C. Multichannel Molecular Switch with a Surface-Confined Electroactive Cl. *Nano Lett.* 4382–4385 (2011).

44. Simão, C. *et al.* A robust molecular platform for non-volatile memory devices with optical and magnetic responses. *Nat. Chem.* **3,** 359–364 (2011).

45. Aviram, A. & Ratner, M. A. Molecular rectifiers. *Chem. Phys. Lett.* **29,** 277–283 (1974).

46. Metzger, R. M. Unimolecular electrical rectifiers. *Chem. Rev.* **103,** 3803–3834 (2003).

47. Metzger, R. M. Unimolecular electronics and rectifiers. *Synth. Met.* **159,** 2277–2281 (2009).

48. Aviram, A., Joachim, C. & Pomerantz, M. Evidence of Switching and Rectification by a Single Molecule Effected with a Scanning Tunneling Microscope. *Chem Phys Lett* **146,** 490–495 (1988).

49. Geddes, N. J., Sambles, J. R., Jarvis, D. J., Parker, W. G. & Sandman, D. J. Fabrication and investigation of asymmetric current-voltage characteristics of a metal / Langmuir – Blodgett monolayer / metal structure. *Appl. Phys. Lett.* **56,** 1916–1918 (1990).

50. Brady, A. C. *et al.* Molecular rectification with M | (D – σ – A LB film) | M junctions. *J. Mater. Chem.* **9,** 2271–2275 (1999).

51. Shumate, W. J. *et al.* Spectroscopy and Rectification of Three Donor - Sigma - Acceptor Compounds, Consisting of a One-Electron Donor (Pyrene or Ferrocene), a One-Electron

Acceptor (Perylenebisimide), and a C 19 Swallowtail. *J. Phys. Chem. B* **110,** 11146–11159 (2006).

52. Ho, G. *et al.* The first studies of a tetrathiafulvalene-σ-acceptor molecular rectifier. *Chem. - A Eur. J.* **11,** 2914–2922 (2005).

53. Metzger, R. M. *et al.* Unimolecular electrical rectification in hexadecylquinolinium tricyanoquinodimethanide. *J. Am. Chem. Soc.* **119,** 10455–10466 (1997).

54. Vuillaume, D., Micro-e, Ä. De, Chen, B. & Metzger, R. M. Electron Transfer through a Monolayer of Hexadecylquinolinium Tricyanoquinodimethanide. **4,** 4011–4017 (1999).

55. Ashwell, G. J., Tyrrell, W. D. & Whittam, A. J. Molecular Rectification : Self-Assembled Monolayers in Which Donor-(π-Bridge)-Acceptor Moieties Are Centrally Located and Symmetrically Coupled to Both Gold Electrodes. *J. Am. Chem. Soc.* **126,** 7102–7110 (2004).

56. Ashwell, G. J., Chwialkowska, A. & High, L. R. H. Rectifying Au–S–C_nH_{2n}–P3CNQ derivatives. *J. Mater. Chem.* **14,** 2848–2851 (2004).

57. Kondratenko, M., Moiseev, A. G. & Perepichka, D. F. New stable donor–acceptor dyads for molecular electronics. *J. Mater. Chem.* **21,** 1470–1478 (2011).

58. Jiang, P., Morales, G. M., You, W. & Yu, L. Synthesis of diode molecules and their sequential assembly to control electron transport. *Angew. Chemie - Int. Ed.* **43,** 4471–4475 (2004).

59. Hihath, J. *et al.* diode with controlled orientation. *Nat. Chem.* **11,** 635–641 (2009).

60. Kornilovitch, P. E., Bratkovsky, A. M. & Williams, R. S. Current rectification by molecules with asymmetric tunneling barriers. *Phys. Rev. B* **66,** 1–11 (2002).

61. Liu, R., Ke, S., Yang, W. & Baranger, H. U. Organometallic molecular rectification. *J. Chemi* **124,** 1–5 (2006).

62. Nijhuis, C. A., Reus, W. F., Barber, J. R., Dickey, M. D. & Whitesides, G. M. Charge transport and rectification in arrays of SAM-based tunneling junctions. *Nano Lett.* **10,** 3611–3619 (2010).

63. Mugnaini, V. *et al.* Looking Inside the Perchlorinated Trityl Radical/Metal Spinterface through Spectroscopy. *J. Phys. Chem. Lett.* **6**, 2101–2106 (2015).

64. Ph.D. Thesis of Dayana Morales. *Article in preparation*.

Publication #6

Title: Grafting TTF-PTM dyads on Surfaces: Towards New Molecular Rectifiers and Switches

Authors: Manuel Souto, Li Yuan, Imma Ratera, Christian A. Nijhuis, and Jaume Veciana

Publication: *In preparation*

Grafting TTF-PTM dyads on Surfaces: towards New Molecular Rectifiers and Switches

Manuel Souto,[†] Li Yuan,[‡] Imma Ratera,[†] Christian A. Nijhuis,[‡] and Jaume Veciana[†]

[†] Institut de Ciència de Materials de Barcelona (ICMAB-CSIC)/CIBER-BBN, Campus Universitari de UAB, 08193 Cerdanyola del Vallès (Barcelona), Spain

[‡] Department of Chemistry, National University of Singapore, 3 Science Drive 3, Singapore 117543, Singapore

ABSTRACT: This article report the self-assembled monolayer (SAM) preparation of the donor-acceptor (D-A) system formed by a tetrathiafulvalene (TTF) moiety linked to a polychlorotriphenylmethyl (PTM) radical unit (**1**) and its non-radical precursor (**2**) on gold. An exhaustive characterization of the SAMs by cyclic voltammetry (CV), X-ray photoemission spectroscopy (PES) and Near-edge X-ray absorption (NEXAFS) is reported. Moreover, ultraflat surfaces of gold (Au^{TS}) supported these SAMs and a eutectic alloy of gallium and indium (EGaIn), covered with a skin of gallium oxide formed electrical contacts with them. The difference on the rectification behavior observed for the two dyads is discussed according to the delocalization of the molecular orbitals.

SECTION: Donor-Acceptor, Self-assembled Monolayers, TTF, PTM radical, Molecular rectifiers

During the last decades there has been a large interest in anchoring functional organic molecules onto solid supports in order to fabricate advanced molecular-controlled electronic devices giving rise to new materials with unprecedented performance. For this purpose, bistable molecules, that undergo chemical or physical changes upon optical, magnetic or electric external stimuli, can serve as active-components for data-storage devices.[1] Fox example, molecular switches based on self-assembled monolayers (SAMs) containing electroactive organic radicals could open new opportunities in this field since it is possible to exploit optical and magnetic responses to an external stimulus. In this direction, polychlorotriphenylmethyl (PTM) radical has been widely use in our group to prepare SAMs on different kind of surfaces due to their potential application as robust molecular platform for memory devices.[2–9] On the other hand, tetrathiafulvalene (TTF) derivatives have been also proposed as building blocks for developing switchable redox systems grafted on surfaces due to the possibility of accessing to three different stable redox states (*i.e.* neutral, radical cation and dication species) with different physic-chemical properties. For example, TTF-based SAMs have been proposed to develop ion sensors and memory devices.[10–18]

On the other hand, dyads formed by an electron donor unit (D) linked to an electron acceptor (A) unit by an organic bridge are very promising materials that have attracted a great deal of attention for applications in molecular electronics as molecular switches and rectifiers. Aviram and Ratner proposed in 1974 the first molecular rectifier that consisted on the electron-donor TTF unit connected to the electron-acceptor TCNQ through an insulating σ-bridge.[19] It passed 25 years until this idea was experimentally confirmed by Metzer and coworkers[20] and, since then, several examples of donor-acceptor dyads have been proposed for developing molecular rectifiers, as monolayers as well as single-molecule junctions.[21–24] In order to study the charge transport mechanism through SAMs, it has been reported junctions based on eutectic alloy of gallium and indium (EGaIn) as top electrode, and ultraflat surfaces of Au or Ag as bottom electrodes.[25,26]

We have recently reported a D-A system consisting on a PTM radical unit linked through a vinylene bridge to a TTF moiety that exhibits bistability in solution.[27–29] In view of its interesting properties and for incorporating these systems on solid platforms, herein we report for the first time the synthesis of the same TTF-π-PTM dyad functionalized with a cyclic disulfide (**1**) that has been used to prepare SAMs on gold. Moreover, the non-radical precursor (**2**), with the same molecular structure but different electronic structure, has been also obtained to study the influence of the open- and close-shell character (Figure 1). An exhaustive characterization of the SAMs by X-ray photoemission and absorption is reported. Moreover, EGaIn junctions have been used to study and discuss the electron transport through SAMs of **1**and **2** that exhibit different rectification behavior.

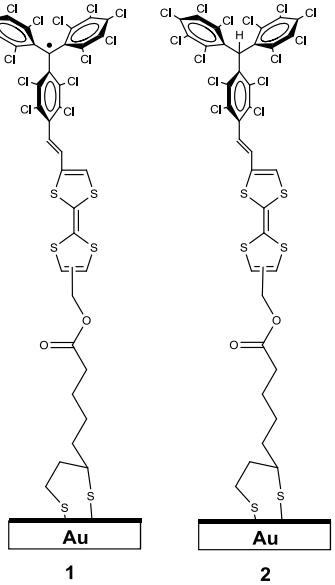

1 **2**

Figure 1. Idealized schematic representation of self-assembled monolayers formed by **1** (**SAM 1**) and **2** (**SAM 2**) on gold.

Results and Discussion

1. Preparation of compound 1 and SAMs

Compound **1** was prepared as outlined in Figure 2. First, compound **5** was obtained through a Wittig-Horner-Emmons reaction between the formyl-hydroxymethyl-TTF (**3**)[30] and the phosphotaned PTM derivative (**4**)[31] in a 33 % yield. The strong stereoselectivity of this reaction gave place to the *trans* isomer of the vinylene bridge. Then, the subsequent deprotonation of **5** with tetrabutylammonium hydroxide (TBAOH) and the oxidation of the generated carbanion with silver nitrate gives **6** in 57 % yield. Finally, the radical **1** was obtained through an esterification reaction between the methyl alcohol **6** and the (±)-α-lipoic acid in a 55 % yield. On the other hand, the esterification reaction between the methyl alcohol **5** and the (±)-α-lipoic acid gave compound **2** in a 65 % yield as a reddish powder (see Supporting Information).

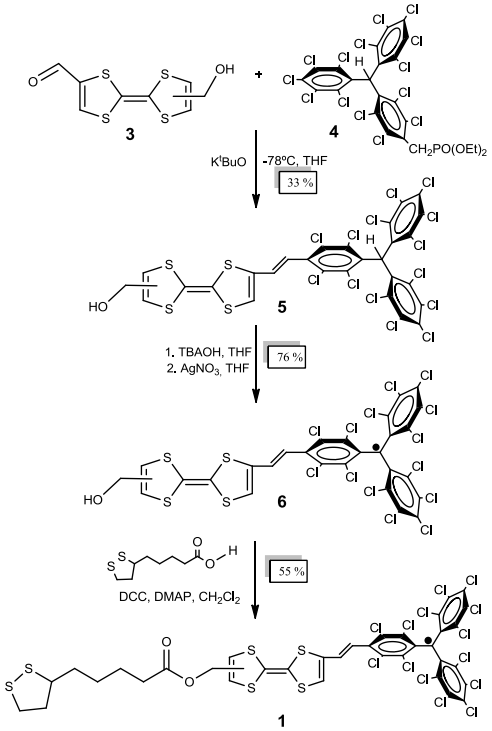

Figure 2. Synthetic route for the preparation of radical dyad **1**.

SAMs of **1** and **2** were prepared following the previously procedure[14] by the immersion of freshly cleaned Au(111) substrates in 1 mM solution of **1** or **2** in toluene under nitrogen atmosphere and in absence of light. The samples were maintained at 40ºC during the first hour and at room temperature for 24-48 h. Then, the functionalized gold substrates were rinsed thoroughly with anhydrous toluene in order to remove any physisorbed material and finally were dried under a nitrogen stream.

2. Characterization of the SAMs

We characterized the SAMs of **1**and **2** by means of ion mass spectrometry (ToF-SIMS), electron spin resonance (ESR), cyclic voltammetry (CV), X-ray photoelectron spectroscopy (XPS) and near edge X-ray absorption (NEXAFS).

ToF-SIMs

ToF-SIMs measurements of SAMs were performed in order to demonstrate the presence and anchoring of compounds **1** and **2** to the Au surface. The mass spectrum obtained is shown in Figure S6 that shows the highest m/z fragment detected for the SAMs at MW=1171 g/mol corresponding to the entire molecule.

ESR

The magnetic character of the radical molecules grafted on the **SAM 1** was also checked by ESR spectroscopy. The ESR spectrum (Figure S7) shows a signal at g = 2.0032 with a linewidth (δH) of 5.2 Gauss.

Cyclic voltammetry

Figure 3 shows cyclic voltammetry (CV) of SAMs on Au derived from **1** and **2**. The experiments were carried out with the standard setup using the functionalized substrate as working electrode and solid silver and platinum wires as reference and counter electrode, respectively, and Fc/Fc^+ was used as internal reference. In the case of **SAM 1** we observed three reversible redox processes at -0.18, 0.48 and 0.78 V that are assigned to the reduction of the PTM radical unit and to the oxidation of the TTF moiety to $TTF^{+\cdot}$ and TTF^{2+}, respectively (See Figure 4). On the other hand, CV of **SAM 2** showed only two reversible redox peaks at 0.49 and 0.78 eV as the non-radical PTM moiety is not an electroactive species anymore. In the two cases the oxidation and reduction peaks were separated by less than 100 mV, as expected for a diffusion controlled processes in SAMs.

a)

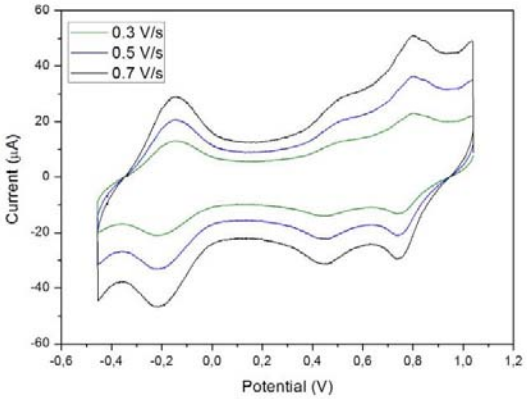

b)

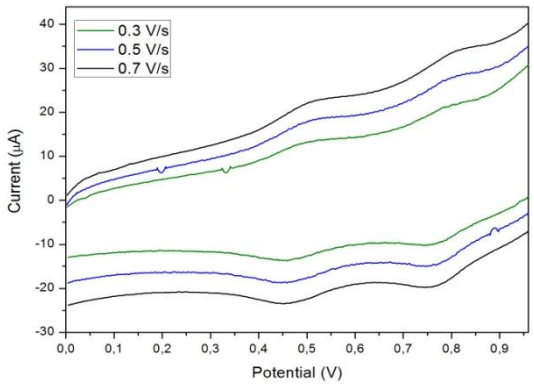

Figure 3. Cyclic voltammetries of a) **SAM 1** and b) **SAM 2** on Au as working electrode, Pt as counter electrode, and Ag/AgCl as reference electrode, recorded at different scan rates with 0.1M $LiClO_4$ solution in acetonitrile as electrolyte.

Table 1. Properties of Self-Assembled Monolayers.

	CV		UPS		NEXAFS		XPS	
SAM	$E_{1/2}^{ox1}$	E_{HOMO} (eV)[a]	**WF (eV)**	E_{HOMO} (eV)[b]	**SUMO (eV)**	**LUMO (eV)**	***d* (nm)[c]**	Γ_{SAM} ($\times 10^{-10}$ mol/cm^2)[d]
1	0.48	-4.98	4.30	-5.25	-3.3	N.A.	2.1	1.16
2	0.49	-4.99	4.34	-5.14	N.A.	-2.80	2.1	1.26

[a] HOMO energies values were calculated from CV data as detailed in the Supporting Information (SI). [b] HOMO energies calculated from UPS as detailed in the SI. The error is 0.05 eV, which is the resolution of the UPS. [c] Thickness of SAMs calculated as detailed in the SI. [c] Surface coverage calculated as detailed in the SI.

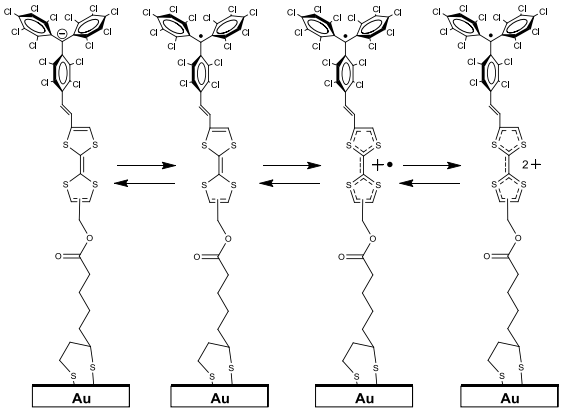

Figure 4. Schematic representation of the four different electrochemical states of **SAM 1**.

XPS

SAMs of **1** and **2** were characterized by X-ray photoelectron spectroscopy (XPS) to determine its electronic structure. The fitting of the C1s spectra (Figure S8a) gives us four principal peaks for both SAMs at 284.8, 285.8, 286.8 and 288.7 eV that are attributed to the aliphatic/aromatic, C-S, chlorinated and carbonyl carbon atoms, respectively. On the other hand, the S2p spectrum showed two doublet characteristics of the sulfur $S2p_{3/2}$ and $S2p_{1/2}$ attributed to the S-Au bond and the sulfurs of the TTF moiety (Figure S8b).[16] The intensity ratio between these two doublets is 1.7:4.4 and 1.8:4.2 for S1 and S2 respectively, close to the theoretical value 2:4. The Cl_{2p} spectra of both SAMs (Figure S8c) showed a doublet with $Cl_{2p3/2}$ binding energy at 200.8 eV (C-Cl) and a spin orbit coupling between $Cl_{2p3/2}$ and $Cl2p_{1/2}$ equal to 1.7 eV. These features are characteristic of the PTM subunit as has been observed for other PTM radicals monolayers.[3,7] Au_{4f} high resolution spectra of both monolayers (Figure S8d) showed the expected doublet at 84 eV ($Au_{4f\ 7/2}$) and 87.7 eV ($Au_{4f\ 5/2}$) and gave us information about the thickness of the SAMs.

Valence Band

Figure 5 shows the valence band spectra of **SAMs 1** and **2** and the cutoff of the HOMO peak near the Fermi Edge. The peaks that appear at lower energy (0.5-1.0 eV) have been attributed to the HOMO orbital that is mainly localized on the electron-donor TTF moiety. At higher energies, we also observed other bands at 3.3 eV, 7.4 ev and 9.1 eV related to other occupied molecular orbitals localized in the PTM units which have been also observed in other similar PTM-based systems.[32]

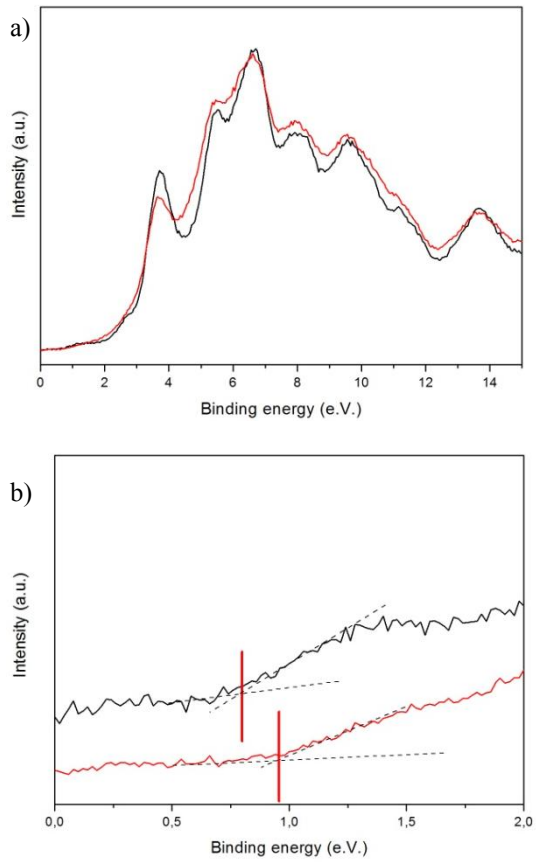

Figure 5. a) Valence band spectra of **SAM 1** (black line) and **SAM 2** (red line) and b) cutoff of the HOMO peak.

NEXAFS

NEXAFS of C *K*-edge was performed for monolayers of **1** and **2** at normal (90º) and grazing (20º) incidence (Figure 6). Both spectra showed an intense peak at 286.4 eV that has been assigned as C(Ph) → π^* resonance on the perchlorinated benzene rings.[32] The main difference between NEXAFS spectra of **SAM 1** and **SAM 2** was the small peak at 282.6 eV observed in the open-shell monolayer (**1**) and absent in the closed-shell protonated monolayer (**2**). This peak has been assigned to the single unoccupied molecular orbital (SUMO)[31] of the PTM radical units. At higher energy the peaks around 289 eV and 288.4 eV can be attributed to C1s transitions into the π^* orbital of the carboxyl group.

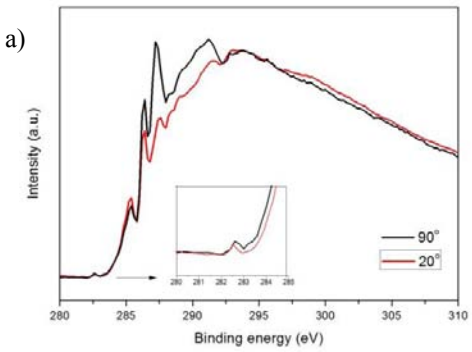

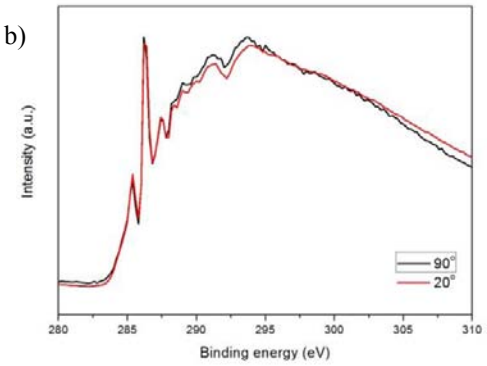

Figure 6. NEXAFS spectra of a) **SAM 1** and b) **SAM 2** in normal (NI, red line, 90º) and grazing (GI, black line, 20º) incidences. Input shows the zoom in the 280-285 eV region.

3. Charge transport measurements

Stable and reproducible molecular junctions based on **SAMs 1** and **2** were prepared on template-stripped gold (Au^{TS}) surface, used as a bottom electrode, and an eutectic indium-gallium (EGaIn) metallic alloy, with a surface layer of Ga_2O_3, as the top contact.[25,26] Charge transport measurements through SAMs were measured with a bias voltage ranged from +2.0 to -2.0 V (Figure 7). Moreover, large numbers of data were acquired and a statistical analysis of them was made in order to discard any artifact from the real data and from imperfections.

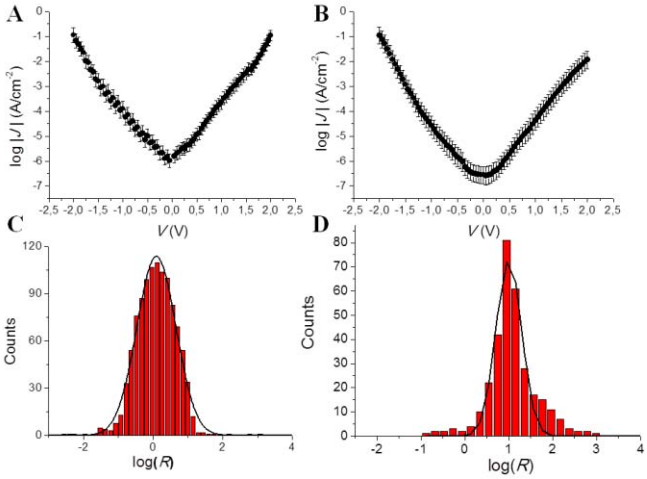

Figure 6. *Top*: Absolute current densities, J (A/cm^2), plotted vs voltages (*V*) of the junctions a) **Au_{TS}-SAM1//Ga_2O_3/EGaIn**, b) **Au_{TS}-SAM2//Ga_2O_3/EGaIn**. *Bottom*: Histogram with a Gaussian fit of the R of the junctions for c) **SAM 1** and d) **SAM 2**.

The most remarkable difference between the charge transport measurements for the two systems was the rectification properties (Table 2). Junctions of **Au-SAM1//Ga_2O_3/EGaIn** didn't show any rectification behavior in the +2.0 to -2.0 V range whereas measurements of **Au-SAM2//Ga_2O_3/EGaIn** showed a moderate rectification ratio ($R = |J(-V)| / |J(V)|$ at $|V|$=2.0 V) of ~13 at $|V|$=2.0 V.

Table 2. Statistical data obtained for the I-V measurements of Au-**SAM 1**//Ga_2O_3/EGaIn and Au-**SAM 2**//Ga_2O_3/EGaIn junctions.

Parameter	**SAM 1**	**SAM 2**
Number of junctions	**22**	**25**

Number of shorts	**4**	**3**
Number of traces	**487**	**528**
Noshorting junctions (%)[a]	**81**	**88**
Rectification ratio (δlog)[b]	**1.2(0.6)**	**12.7 (0.7)**

It is important to note that one of the keys for obtaining rectification behavior in D-A systems is to have an effective separation between the HOMO and LUMO orbitals through a bridge.[23] Thus, the difference between both systems can be to the higher HOMO delocalization of the TTF moiety through the PTM radical in **1** in comparison with **2**. This overlap between the donor and acceptor units in **1** is in agreement with the intramolecular charge transfer (ICT) band observed in the absorption spectrum (Figure S3).

Conclusions

In summary, we have reported for the first time the preparation of self-assembled monolayers on gold of the D-A system based on the electron-acceptor PTM radical linked to the electron-donor TTF unit by a vinylene bridge. Moreover, an exhaustive characterization of the SAMs by cyclic voltammetry and photoelectron spectroscopy were performed in order to determine the energy values of the HOMO and LUMO values localized on the donor and acceptor moieties, respectively. Finally, EGaIn junctions with SAMs of **1** didn't show any rectification behavior whereas junctions with SAMs of **2** showed a moderate rectification ratio of ~13 at |V|=2.0 V. This difference could be attributed to the higher delocalization of the HOMO orbital of TTF through the PTM radical in **1** in comparison with **1-H**. These D-A radical systems anchored in surfaces are very promising molecular building blocks for the development of new molecular switches and rectifiers on surfaces.

ACKNOWLEDGMENT

This work was supported by the DGI grant (POMAs (CTQ2010-19501), the Networking Research Center on Bioengineering, Biomaterials, and Nanomedicine (CIBER-BBN), and the Generalitat de Catalunya (grant 2009SGR00516). M.S. is grateful to MEC for a FPU predoctoral grant and he is enrolled in the Material Science Ph.D. program of UAB.

References

(1) Balzani, V.; Credi, A.; Venturi, M. *Molecular Devices and Machines: Concepts and Per-spectives for the Nanoworld*; Wiley-VCH: Weinheim: Germany, 2008.

(2) Crivillers, N.; Mas-Torrent, M.; Perruchas, S.; Roques, N.; Vidal-Gancedo, J.; Veciana, J.; Rovira, C.; Basabe-Desmonts, L.; Ravoo, B. J.; Crego-Calama, M.; Reinhoudt, D. N. *Angew. Chemie - Int. Ed.* **2007**, *46* (13), 2215–2219.

(3) Shekhah, O.; Roques, N.; Mugnaini, V.; Munuera, C.; Ocal, C.; Veciana, J.; Wöll, C. *Langmuir* **2008**, *24* (13), 6640–6648.

(4) Crivillers, N.; Mas-Torrent, M.; Vidal-Gancedo, J.; Veciana, J.; Rovira, C. *J. Am. Chem. Soc.* **2008**, *130* (16), 5499–5506.

(5) Crivillers, N.; Munuera, C.; Mas-Torrent, M.; Simão, C.; Bromley, S. T.; Ocal, C.; Rovira, C.; Veciana, J. *Adv. Mater.* **2009**, *21* (10-11), 1177–1181.

(6) Mas-Torrent, M.; Crivillers, N.; Mugnaini, V.; Ratera, I.; Rovira, C.; Veciana, J. *J. Mater. Chem.* **2009**, *19* (12), 1691.

(7) Simão, C.; Mas-torrent, M.; Veciana, J.; Rovira, C. *Nano Lett.* **2011**, 4382–4385.

(8) Simão, C.; Mas-Torrent, M.; Crivillers, N.; Lloveras, V.; Artés, J. M.; Gorostiza, P.; Veciana, J.; Rovira, C. *Nat. Chem.* **2011**, *3* (5), 359–364.

(9) Mas-Torrent, M.; Crivillers, N.; Rovira, C.; Veciana, J. *Chem. Rev.* **2012**, *112* (4), 2506–2527.

(10) Herranz, M. Á.; Yu, L.; Martín, N.; Echegoyen, L. *J. Org. Chem.* **2003**, *68* (22), 8379–8385.

(11) Liu, S. G.; Liu, H.; Bandyopadhyay, K.; Gao, Z.; Echegoyen, L. *J. Org. Chem.* **2000**, *65* (11), 3292–3298.

(12) Tripp, G.; Oçafrain, M.; Besbes, M.; Monroche, V.; Lyskawa, J.; Le Derf, F.; Sallé, M.; Becher, J.; Colonna, B.; Echegoyen, L. *New J. Chem.* **2002**, *26* (10), 1320–1323.

(13) Simão, C.; Mas-Torrent, M.; Casado-Montenegro, J.; Otón, F.; Veciana, J.; Rovira, C. *J. Am. Chem. Soc.* **2011**, *133* (34), 13256–13259.

(14) Casado-Montenegro, J.; Mas-Torrent, M.; Otón, F.; Crivillers, N.; Veciana, J.; Rovira, C. *Chem. Commun. (Camb).* **2013**, *49* (73), 8084–8086.

(15) Liu, H.; Liu, S.; Echegoyen, L. *Chem. Commun.* **1999**, *100* (16), 1493–1494.

(16) Yokota, Y.; Miyazaki, A.; Fukui, K. I.; Enoki, T.; Tamada, K.; Hara, M. *J. Phys. Chem. B* **2006**, *110* (41), 20401–20408.

(17) Paxton, W. F.; Kleinman, S. L.; Basuray, A. N.; Stoddart, J. F.; Van Duyne, R. P. *J. Phys. Chem. Lett.* **2011**, *2* (10), 1145–1149.

(18) Simao, C.; Mas-Torrent, M.; André, V.; Duarte, M. T.; Veciana, J.; Rovira, C. *Chem. Sci.* **2013**, *4* (1), 307.

(19) Aviram, A.; Ratner, M. A. *Chem. Phys. Lett.* **1974**, *29* (2), 277–283.

(20) Metzger, R. M.; Chen, B.; Hopfner, U.; Lakshmikantham, M. V.; Vuillaume, D.; Kawai, T.; Wu, X.; Tachibana, H.; Hughes, T. V.; Sakurai, H.; Baldwin, J. W.; Hosch, C.; Cava, M. P.; Brehmer, L.; Ashwell, G. J. *J. Am. Chem. Soc.* **1997**, *119* (43), 10455–10466.

(21) Metzger, R. M. *Chem. Rev.* **2003**, *103* (9), 3803–3834.

(22) Metzger, R. M. *Chem. Rev.* **2015**, 150507090420005.

(23) Ho, G.; Heath, J. R.; Kondratenko, M.; Perepichka, D. F.; Arseneault, K.; Pézolet, M.; Bryce, M. R. *Chem. - A Eur. J.* **2005**, *11* (10), 2914–2922.

(24) Kondratenko, M.; Moiseev, A. G.; Perepichka, D. F. *J. Mater. Chem.* **2011**, *21* (5), 1470.

(25) Nijhuis, C. a.; Reus, W. F.; Whitesides, G. M. *J. Am. Chem. Soc.* **2009**, *131* (49), 17814–17827.

(26) Nijhuis, C. a.; Reus, W. F.; Whitesides, G. M. *J. Am. Chem. Soc.* **2010**, *132* (51), 18386–18401.

(27) Guasch, J.; Grisanti, L.; Lloveras, V.; Vidal-Gancedo, J.; Souto, M.; Morales, D. C.; Vilaseca, M.; Sissa, C.; Painelli, A.; Ratera, I.; Rovira, C.; Veciana, J. *Angew. Chemie - Int. Ed.* **2012**.

(28) Guasch, J.; Grisanti, L.; Souto, M.; Lloveras, V.; Vidal-Gancedo, J.; Ratera, I.; Painelli, A.; Rovira, C.; Veciana, J. *J. Am. Chem. Soc.* **2013**.
(29) Souto, M.; Guasch, J.; Lloveras, V.; Mayorga, P.; López Navarrete, J. T.; Casado, J.; Ratera, I.; Rovira, C.; Painelli, A.; Veciana, J. *J. Phys. Chem. Lett.* **2013**.
(30) Terkia-derdra, N.; Andreu, R.; Salle, M.; Levillain, E.; Orduna, Â.; Garín, J.; Ortí, E.; Viruela, R.; Sahraoui, B.; Gorgues, A.; Favard, J. *Chem. Eur. J.* **2000**, *7*, 1199–1213.
(31) Rovira, C.; Ruiz-Molina, D.; Elsner, O.; Vidal-Gancedo, J.; Bonvoisin, J.; Launay, J. P.; Veciana, J. *Chemistry* **2001**, *637–639*, 251–257.
(32) Mugnaini, V.; Calzolari, A.; Ovsyannikov, R.; Vollmer, A.; Gonidec, M.; Alcon, I.; Veciana, J.; Pedio, M. *J. Phys. Chem. Lett.* **2015**, 2101–2106.

Supporting Information

Four-State Surface-Confined Molecular Switch based on a TTF-PTM Radical

Contents

1. General methods for synthesis and characterization
2. Synthesis and characterization of **1** and **2**
3. General procedures for the device preparation and characterization
4. References

1. General methods for synthesis and characterization

All reagents and solvents employed for the syntheses were of high purity grade and were purchased from Sigma-Aldrich Co., Merck, and SDS. Dry solvents were used in the chemical reactions and in the cyclic voltammetries. Chlorinated solvents were filtered with basic alumina in order to deactivate the acidic points. ^{1}H NMR spectra were recorded using a Bruker Avance 250, 400, or 500 instruments and Me_4Si as an internal standard. Infrared spectra were recorded with Spectrum One FT-IR Spectroscopy instrument and UV/Vis/NIR spectra were measured using Cary 5000E Varian. ESR spectra were performed with a Bruker ESP 300 E equipped with a rectangular cavity T102 that works with an X-band (9.5 GHz). The solutions were degassed by argon bubbling before the measurements. LDI/TOF MS were recorded in a Bruker Ultraflex LDI-TOF spectrometer. Cyclic voltammetry measurements were obtained with a potentiostat 263a from EG&G Princeton Applied Research in a standard 3 electrodes cell. The IR-NIR spectra have been collected with a Bruker FT-IR IFS-66 spectrometer equipped with a Hyperion microscope. The spectral resolution is about 2 cm^{-1} for both spectrometers. TOF-SIMs measurements of SAMs were recorded using a primary gun that was bombardment with Bi ions with the following intensities: 1.2 pA (Bi^+), 0.3 pA ($Bi^{+\,3}$, 0.2 pA ($Bi^{++\,3}$).

2. Synthesis and characterization of 1 and 2

Synthesis of 3

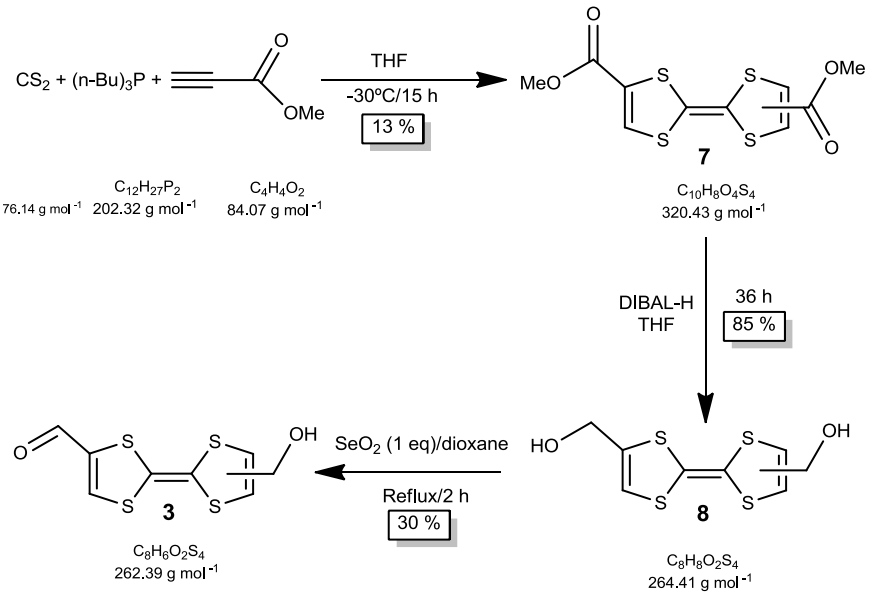

Synthesis of 7

Tributylphosphine (20.3 g, 0.1 mol) was added dropwise to a solution of 10 ml of carbon disulfide in 50 ml of tetrahydrofuran at -10ºC under inert conditions and the deep maroon solution was stirred at room temperature for 1 hour. Next the mixture was cooled to -40ºC and a solution of methyl propiolate (8.4 g, 0.1 mol) in 20 ml of tetrahydrofuran was added dropwise. The temperature was maintained between -30ºC and -50ºC during the addition. The solution was warmed to room temperature and stirred overnight. Finally solvents were evaporated under reduced pressure, the residue was stirred with ether to crash out the product that and was filtered and washed with Et_2O to give 4.2 g (13 %) of the red microcrystalline powder **7**. **Characterization**: **^{1}H-NMR** (250 MHz, $CDCl_3$, δ(ppm): 7.35 (d, 2H, CH, J = 7.34 Hz); 3.82 (s, 6H, CH_3). **FT-IR** (ν cm^{-1}): 2956 (w); 2922 (w); 2852 (w); 1712 (s, C=O); 1548 (s); 1434 (m); 1244 (s); 1199 (m); 1045 (m); 940 (m); 829 (m); 820 (m); 763 (m); 725 (m). **LDI-TOF** (positive mode): *m/z* (amu/e^-): 320.377 ($M^{+\cdot}$).

Synthesis of 8

30 ml of DIBAL-H (1 M in THF) was added dropwise to a solution of 4,4'(5')-Bis(methoxycarbonyl) tetrathiafulvalene (**7**) (1 g, 3.12 mmol) in 60 ml of tetrahydrofuran cooled at -70ºC under strict inert conditions. The color of the solution changes from red to yellow during the first hour of reaction. Then the solution was allowed to warm to room temperature and stirred overnight. The absence of TTF diester was confirmed by TLC and the reaction was hydrolyzed by the carefully addition of 10 ml of MeOH/HCl 12 M (3:1) mixture to the solution previously cooled with an ice bath. Then ether was added to the mixture and the organic phase was washed with three portions of water (100 ml), dried with anhydrous $MgSO_4$ and solvents were evaporated under reduced pressure. Finally the product was purified by column chromatography of silica gel using a mixture of ether and hexane to obtain 738 mg (85 %) of TTF diol **8** as a light brown solid. **Characterization**: **^{1}H-NMR** (250 MHz, DMSO-D_6, δ(ppm): 6.52 (s, 2H, CH); 5.48 (t, 2H, *J* = 5.9 Hz); 4.20 (d, 4H, *J* = 5.84 Hz, **CH_2**OH). **FT-IR** (ν cm^{-1}): 3338 (s, OH); 3256 (s, OH); 2947 (m); 2918 (m); 2858 (m); 1587 (w); 1459 (m); 1443 (m); 1430 (m); 1369 (m); 1228 (m); 1092 (s); 1012 (s); 969 (m); 839 (w); 773 (w); 741 (w) 709 (w). **LDI-TOF** (positive mode): *m/z* (amu/e^-): 263.926 ($M^{+\cdot}$).

Synthesis of 3

A solution of equimolar amounts of 2,6(7)-bis(hydroxymethyl)-TTF (**8**) (750 mg, 2.84 mmol) and selenium dioxide (315 mg)was heated under reflux for 2 h in dry dioxane (70 mL); the solution turned from yellow to dark red. Cooling of the solution resulted in the formation of a black precipitate of elemental selenium, which was filtered and washed thoroughly with dichloromethane. The solvent mixture was then evaporated under reduced pressure to produce a dark red oil, which was purified by SiO_2 column chromatography (eluent: hexane: Et_2O) to afford a fraction that corresponds to the 2-formyl-6(7)-hydroxymethyl TTF (**3**) (220 mg, 30%) as a violet microcrystalline powder. **Characterization**: **^{1}H-NMR** (250 MHz, DMSO-D_6, δ(ppm): 9.53 (s, 1H, CHO); 8.26 (s, 1H); 6.60 (s, 1H); 5.55 (t, *J* = 5.2 Hz, 1H, OH); 4.23 (d, 2H, *J* = 5.2 Hz, CH_2OH). **FT-IR** (ν cm^{-1}): 3405 (m, OH); 2918 (m); 2851 (m); 1721 (w); 1625 (s, C=O); 1540 (m); 1512 (s); 1363 (m); 1280 (w); 1230 (m); 1140 (s); 1109 (m); 1010 (m); 954 (m); 839 (s); 747 (m). L**DI-TOF** (positive mode): *m/z* (amu/e^-): 261.976 ($M^{+\cdot}$).

Synthesis of 1

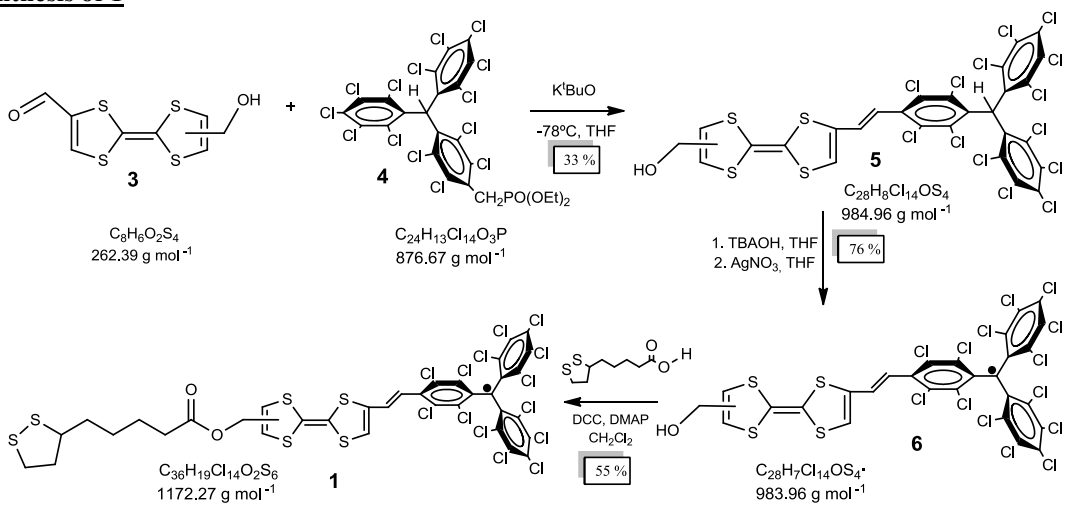

Synthesis of 5

600 mg (0.68 mmol) of the phosphonated PTM derivative (**4**) were dissolved in 50 ml of anhydrous THF under strict inert conditions. The solution was cooled down to -78 ºC. Next, 130 mg (1.15 mmol) of potassium *tert*-butoxide were added and stirred for 20 minutes to form the yellow-orange ylide. Then 195 mg (0.75 mmol) of 2-formyl-6(7)-hydroxymethyl tetrathiafulvalene (**3**) were added and the reaction was warmed up to room temperature and stirred for 2 days. Then the mixture was washed with water, dried

with anhydrous $MgSO_4$ and solvents were evaporated under reduced pressure. Finally the product was purified by column chromatography of silica gel using a mixture of ether and hexane to obtain to obtain 220 mg (33 %) of hydroxymethyl-TTF-PTMαH (**5**) as a red powder. **Characterization**: **^{1}H-NMR** (250 MHz, DMSO-D_6, δ(ppm): 7.18 (s, 1H, αH); 7,14 (d, *J* = 16.1 Hz, 1H, CH=CH); 6.91 (s, 1H, C**H**=C-CH=CH); 6.58 (s, 1H, C**H**=C-CH_2OH); 6.31 (d, *J* = 16.2 Hz, CH=CH); 5.33 (t, *J* = 5.53 Hz, 1H, OH); 4.23 (d, *J* = 4.7 Hz, 2H, C**H_2**OH). **FT-IR** (ν cm^{-1}): 3368 (m, OH); 2956 (m); 2922 (m); 2855 (m); 1614 (m, CH=CH); 1517 (m); 1454 (m); 1357 (s); 1337 (s); 1296 (s); 1188 (w); 1139 (m); 1116 (m); 1019 (m); 941 (m); 862 (w); 808 (s); 776 (m) 750 (s); 713 (m); 682 (m). L**DI-TOF** (positive mode): *m/z* (amu/e^-): 983.515 ($M^{+\cdot}$). **Cyclic voltammetry** (Bu_4NPF_6 0.15 M in CH_2Cl_2 as electrolyte): $E_{½}^1$=0.47 V; $E_{½}^2$=0.97 V.

Synthesis of 6

50 mg (0.05 mmol) of **5** were dissolved in 20 ml of dry THF and 100 μl (0.1 mmol) of tetrabutylammonium hydroxide 1.0 M in water were added and the purple solution was stirred for 40 minutes. Then the reaction mixture was stirred with 17 mg (0.1 mmol) of silver nitrate in THF/AcMe (5:1) for 20 minutes. The solution changes from purple to dark brown with silver (Ag^0) precipitated. Then the solution was filtered and the solvent was evaporated under reduced pressure. Finally, the product was purified by flash column chromatography of silica gel using CH_2Cl_2 as eluent and precipitated with methanol to produce 38 mg of radical **6** (76 %). **Characterization**: **FT-IR** (ν cm^{-1}): 3405 (m, OH); 2955 (m); 2922 (m); 2855 (m); 1728 (w); 1604 (m, CH=CH); 1506 (m); 1460 (m); 1335 (s); 1261 (s); 1160 (w); 1137 (w); 1118 (w); 1029 (m); 940 (m); 865 (w); 817 (m); 774 (w) 754 (w); 735 (m); 709 (m); 696 (w); 680 (w). **UV-VIS-NIR** (CH_2Cl_2, λ_{max} in nm, ε in $M^{-1}\cdot cm^{-1}$): 296 (18087); 319 (16067); 387 (20004); 425 (11174). **LDI-TOF** (positive mode): *m/z* (amu/e^-): 982.793 ($M^{+\cdot}$); (negative mode): 982.796 ($M^{-\cdot}$). **Cyclic voltammetry** (Bu_4NPF_6 0.15 M in CH_2Cl_2 as electrolyte):$E_{½}^1$= -0.188 V; $E_{½}^2$=0.476 V; $E_{½}^3$=0.956 V.

Synthesis of 1

40 mg (0.04 mmol) of **6** and 10 mg thioctic acid (1.2 molar equiv.) were dissolved in 10 mL of distilled CH_2Cl_2 and stirred at 0 °C (ice/water bath) under Ar for 15 min. Then 13 mg (1.5 molar equiv) of 1,3-dicyclohexylcarbodiimide (DCC) and 1.5 mg (0.3 molar equiv) of 4-(dimethylamino)-pyridine (DMAP) were added to the solution and the mixture was stirred for another 15 min at 0 °C. The cooling bath was then removed, and the solution was allowed to warm at room temperature overnight. Next the reaction mixture was washed with water (50 mL) and the organic layer was dried over $MgSO_4$, filtered, and evaporated. The residue was subjected to column chromatography (CH_2Cl_2/Hexane) and precipitated with methanol to obtain 26 mg of radical **1** (55 %). **Characterization**: **FT-IR** (ν cm^{-1}): 2955 (m); 2922 (s); 2855 (s); 1736 (m, C=O); 1662 (w); 1604 (w, C=C); 1554 (w); 1499 (w); 1460 (m); 1372 (w); 1335 (s); 1259 (m); 1159 (w); 1135 (w); 1120 (w); 1028 (w); 940 (m); 865 (w); 817 (m); 776 (w); 735 (w); 708 (w); 693 (w).). **UV-VIS-NIR** (CH_2Cl_2, λ_{max} in nm, ε in $M^{-1}\cdot cm^{-1}$): 293 (16515); 324 (15110); 387 (16555); 425 (9368). L**DI-TOF** (negative mode): *m/z* (amu/e^-): 1171.638 ($M^{-\cdot}$). L**DI-TOF** (positive mode): *m/z* (amu/e^-): 1172.794 ($M^{+\cdot}$); (negative mode): 1172.878 ($M^{-\cdot}$). **Cyclic voltammetry** (Bu_4NPF_6 0.15 M in CH_2Cl_2 as electrolyte):$E_{½}^1$= -0.239 V; $E_{½}^2$=0.477 V; $E_{½}^3$=0.861 V.

Synthesis of 2

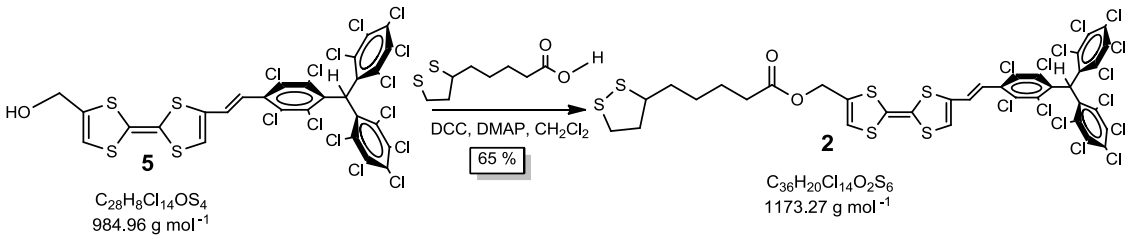

60 mg (0.04 mmol) of **4** and 15 mg thioctic acid (1.2 molar equiv.) were dissolved in 15 mL of distilled CH_2Cl_2 and stirred at 0 °C (ice/water bath) under Ar for 15 min. Then 20 mg (1.5 molar equiv) of 1,3-dicyclohexylcarbodiimide (DCC) and 2.3 mg (0.3 molar equiv) of 4-(dimethylamino)-pyridine (DMAP) were added to the solution and the mixture was stirred for another 15 min at 0 °C. The cooling bath was then removed, and the solution was allowed to warm at room temperature overnight. Next the reaction mixture was washed with water (50 mL) and the organic layer was dried over $MgSO_4$, filtered, and evaporated. The residue was purified by column chromatography (CH**2**Cl**2**/Hexane) and precipitated with methanol to obtain 46 mg of **8** (65 %) as a red powder. **Characterization**: **^{1}H-NMR** (250 MHz C_6D_6, δ(ppm): 7.21 (s, 1H, *α*H); 6,29 (d, *J* = 16.1 Hz, 2H, CH=CH); 6.14 (d, *J* = 16.1 Hz, 2H, CH=CH); 5.52 (s, 1H, TTF); 5.46 (s, 1H, TTF); 4.42 (s, 2H, COO-CH_2-TTF); 3.92-3.78 (m, 1H); 3.61-3.52 (m, 1H); 3.19-3.06 (m, 1H); 2.70-2.54 (m, 2H); 1.97 (td, 7.2, 4.0 Hz, 3H); 1.88-1.74 (m, 3 H); 1.60-1.49 (m, 2H). **FT-IR** (ν cm^{-1}): 2952 (m); 2922 (s); 2851 (s); 1738 (s, C=O); 1614 (m, C=C); 1517 (m); 1456 (m); 1370 (m); 1335 (m); 1296 (m); 1235 (w); 1136 (m); 1020 (w); 943 (m); 862 (w); 808 (s); 774 (m); 754 (m); 696 (w) 683 (w). **UV-VIS-NIR** (CH_2Cl_2, λ_{max} in nm, ε in $M^{-1}\cdot cm^{-1}$): 231 (62565); 305 (22253); 449 (3942). L**DI-TOF** (positive mode): *m/z* (amu/e^-): 1171.39 ($M^{+\cdot}$). **Cyclic voltammetry** (Bu_4NPF_6 0.15 M in CH_2Cl_2 as electrolyte): $E_{½}^1$=0.435 V; $E_{½}^2$=0.891 V; $E_{½}^3$=1.08 (S-S).

^{1}H-NMR of 5

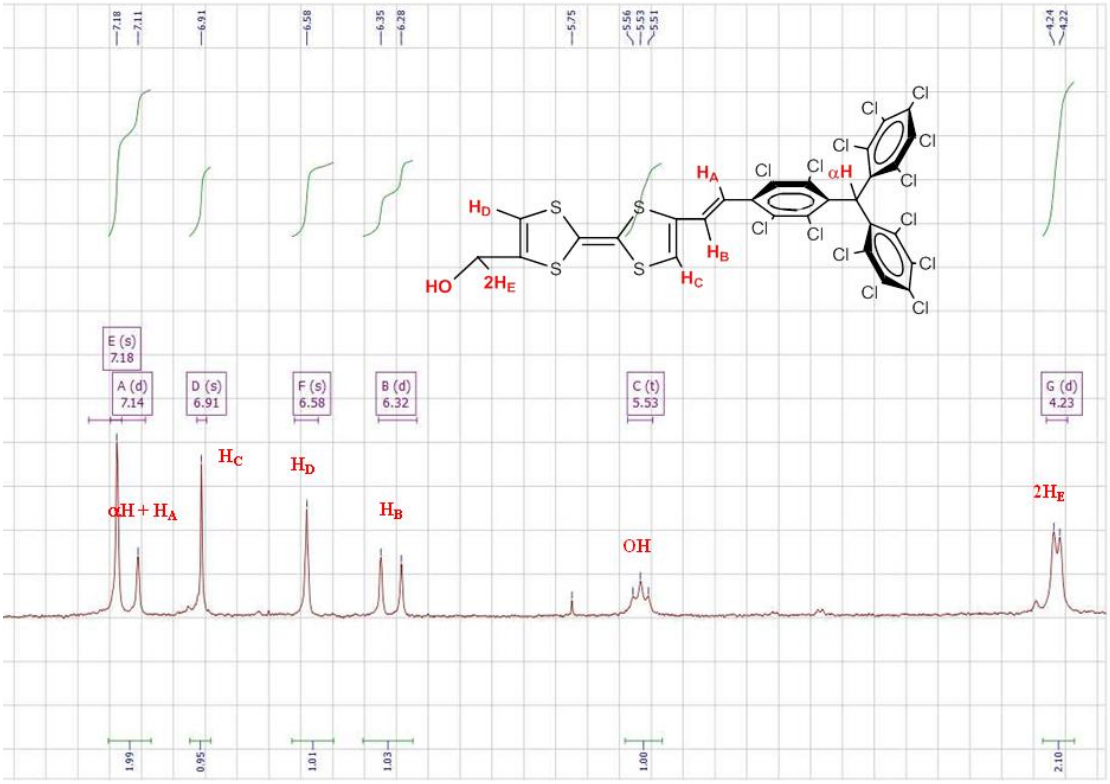

Figure S1. ^{1}H-NMR spectrum of compound **5** in DMSO-D_6 and protons observed in the ^{1}H-NMR spectrum.

^{1}H-NMR of 2

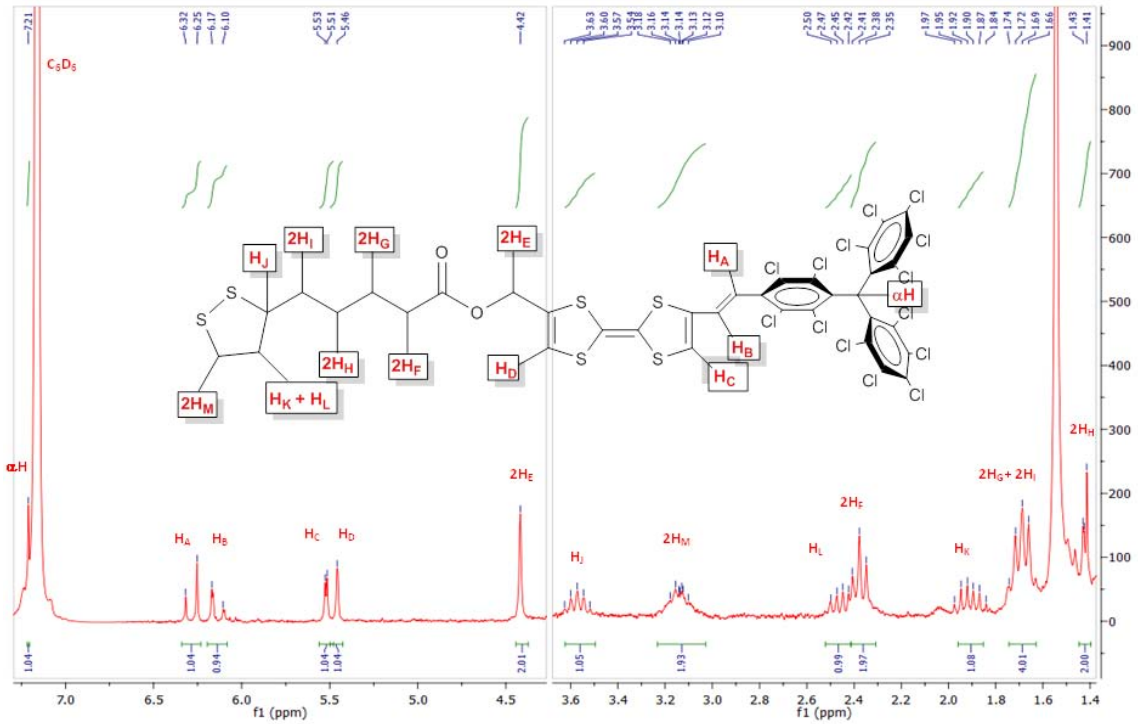

Figure S2. ^{1}H-NMR spectrum of compound **2** in C_6D_6 and protons observed in the ^{1}H-NMR spectrum.

UV-vis-NIR of 1 and2

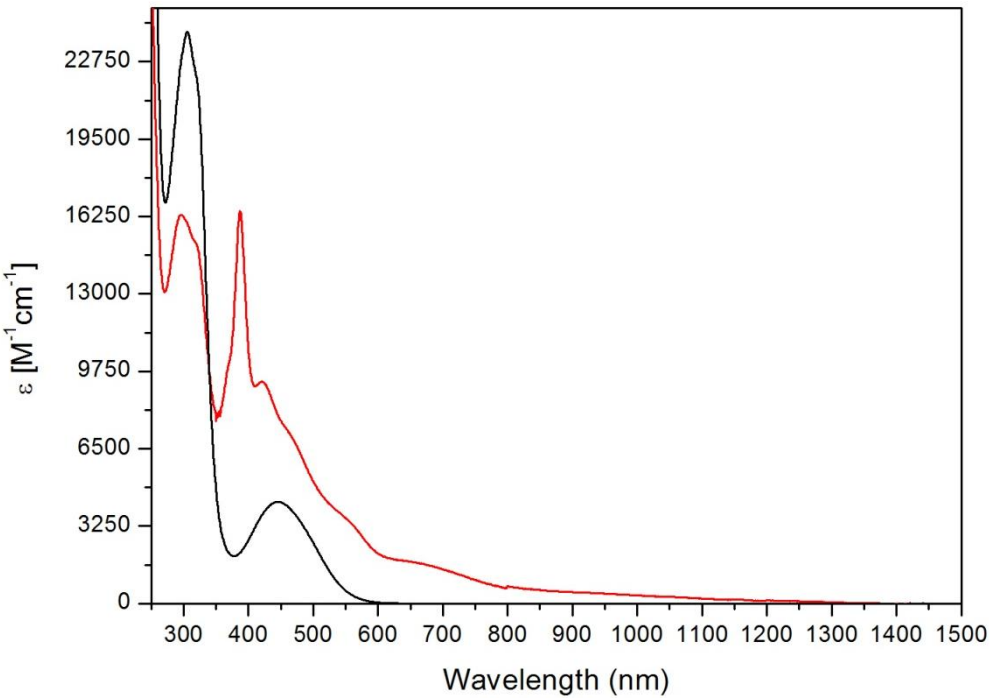

Figure S3. UV-Vis-NIR spectra of a solution 0.05 mM of radical disulfide derivative **1** (red line) and non-radical disulfide derivative **2** (black line) in CH_2Cl_2 at room temperature.

IR of 1 and2

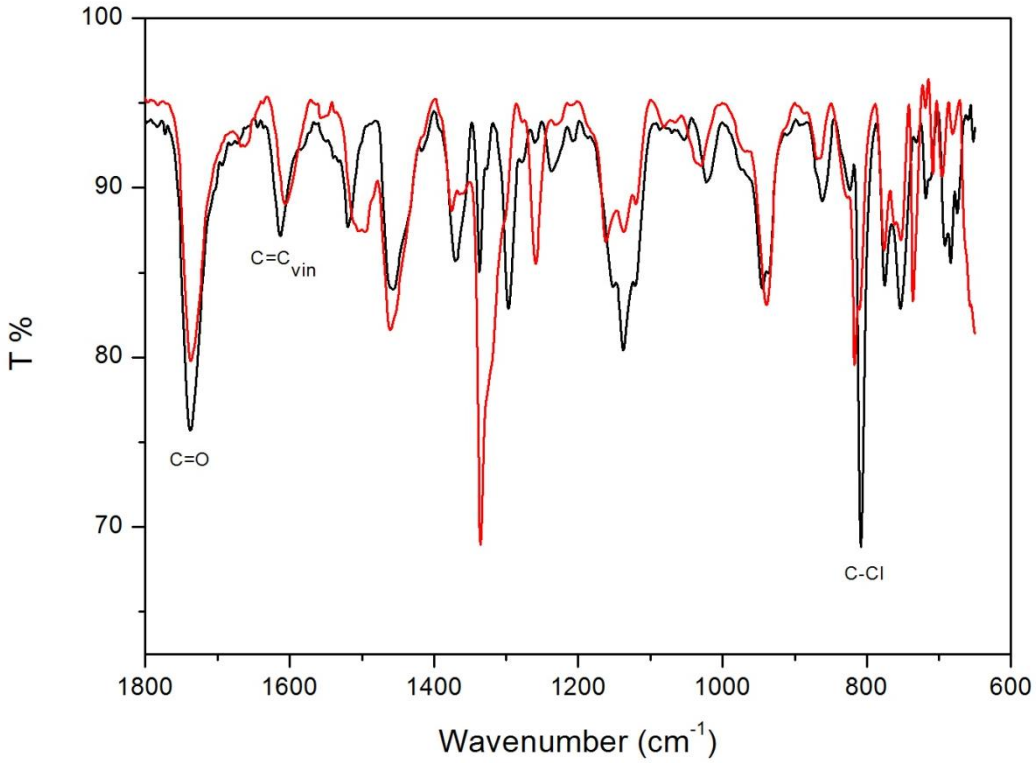

Figure S4. FT-IR spectra of radical disulfide derivative **1** (red line) and non-radical disulfide derivative **2** (black line) in the 1800-600 cm^{-1} region**.**

CV of 1 and2

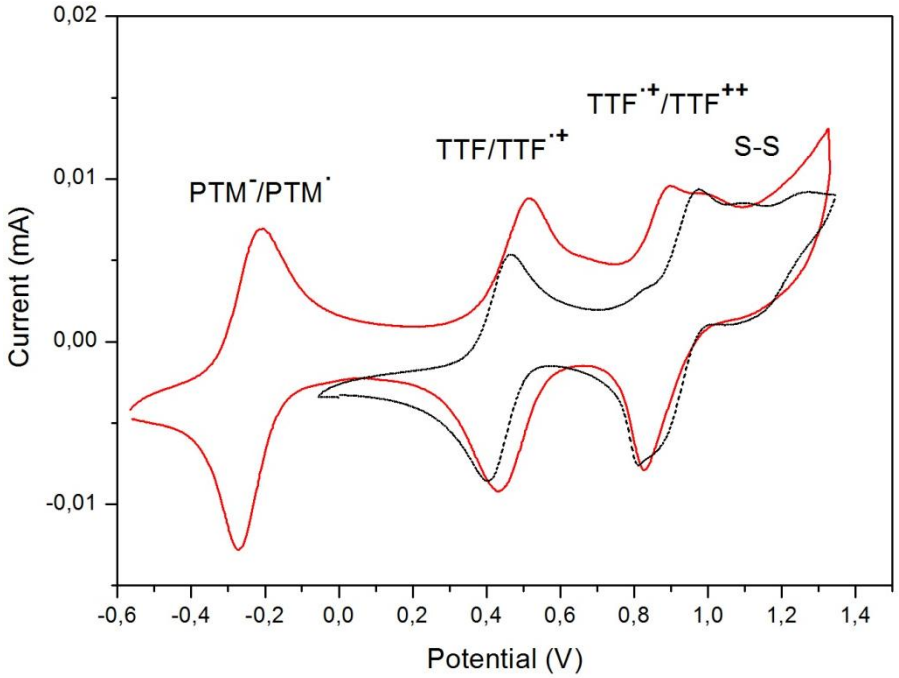

Figure S5. FT-IR spectra of radical disulfide derivative **1** (red line) and non-radical disulfide derivative **2** (black line) in the 1800-600 cm^{-1} region**.**

3. General procedure for the device preparation and characterization

3.1. Ultraflat template surfaces

We have reported the procedure to fabricate the ultraflat Au surfaces by a template-stripping (TS) method where else.[S6] Here, we only give a short description with key experimental factors as follow. We deposited 200 nm thick Au with 99.999% purity (Super Conductor Materials Inc) film on clean Si(100) wafers with their native SiO_2 surface layer by thermal deposition (Shen Yang Ke Yi, China) with a base pressure of 2×10^{-6} mbar. The deposition rate of the first 50 nm thick Au was about 0.3 Å/s and then increased to about 5 Å/s for the rest 150 nm. We used the thermal curable epoxy (EpoTek, 353ND) to glue the clean glass slides on the Au surfaces. The epoxy was cured at at 80 °C for 8 hour in an oven. We only cleaved off the metal surface with glass slide as support from the Si wafer before the immersion of the Au^{TS} surfaces into the thiol solutions, in order to minimize the contamination from air.

3.2. Preparation of the SAMs

Au^{TS} surfaces were immersed in a freshly prepared solution of 1 mM of each compound (**1** or **2**) in toluene (HPLC grade) for initial 24 hours at 40 °C and then for additional 24 hours at room temperature. Always, before immersing the substrates, the solution was degassed with argon. During the SAM formation the solution was kept in dark and under argon atmosphere to avoid the decomposition of the radical species. After the time indicated above, the substrates were removed from the solution and were washed with toluene to remove any physisorbed material. The modified substrates were characterized immediately after being removed from the solution

3.3. Electrochemical characterization of the SAMs

The two SAMs (**1** and **3**) were electrochemically characterized by using cyclic voltammetry (CV) performed with an AUTOLAB 204 with NOVA 1.9 software. We used a custom built electrochemical cell with a Pt-wire as counter electrode, Ag-wire as pseudo reference electrode and the modified Au(111) on mica as working electrode. The area exposed to the lithium perchlorate ($LiClO_4$) in acetonitrile electrolyte solution (0.1 M) was 0.26 cm^2. The CVs were recorded in the range from -0.5 V to 1.0 V. The electrochemical measurements were performed in a Faraday cage.

3.4. ToF-SIMs of 1

We performed ToF-SIMs measurements in order to demonstrate the presence and anchoring of compound **1** to the Au surface. The mass spectra obtained are shown in Figure S1 where the highest m/z fragment detected for SAMs of **1** was the one corresponding to the entire molecule (MW=1172 g/mol).

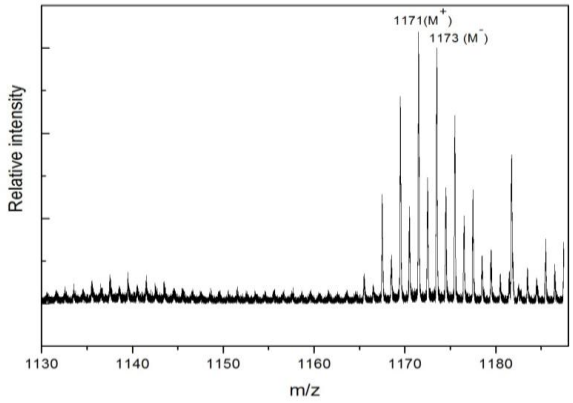

Figure S6. Positive mode ToF-SIMS mass spectrum of **SAM** derived from **1**. Zoom of the specific region showing the highest m/Z fragment detected for SAMs of **1** corresponding to the entire molecule (MW=1154 g/mol).

3.5. ESR of 1

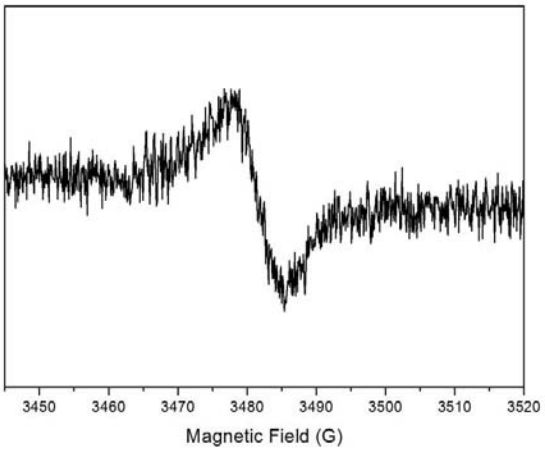

Figure S7. EPR spectra of SAMs of **1**.

3.6. Photoelectron spectroscopy

Photoemission spectroscopy (PES) measurements (including X-ray and ultraviolet photoelectron spectroscopy) and near edge X-ray absorption fine structure (NEXAFS) spectroscopy were performed at the MBS (Materials Science Beamline) of Elettra Synchrotron (Trieste, Italy). We used the Au $4f_{7/2}$ core level peak at 84.0 eV measured from a sputter-cleaned gold foil in electrical contact with the sample to calibrate the photon energy. We chose 500 eV to probe the Cl 2*p*, S 2*p* and C 1*s*, and 40 eV for the valence band measurements. To measure the work function, we applied –10 V bias to the sample to overcome the work function of the analyzer. All UPS spectra were referenced to the Fermi edge of Au and all PES spectra were normalized by the photon current. For NEXAFS, we measured the photon energy from 270 eV to 330 eV. Two take-off angles (90° and 20°) were used to probe the angle-dependence.

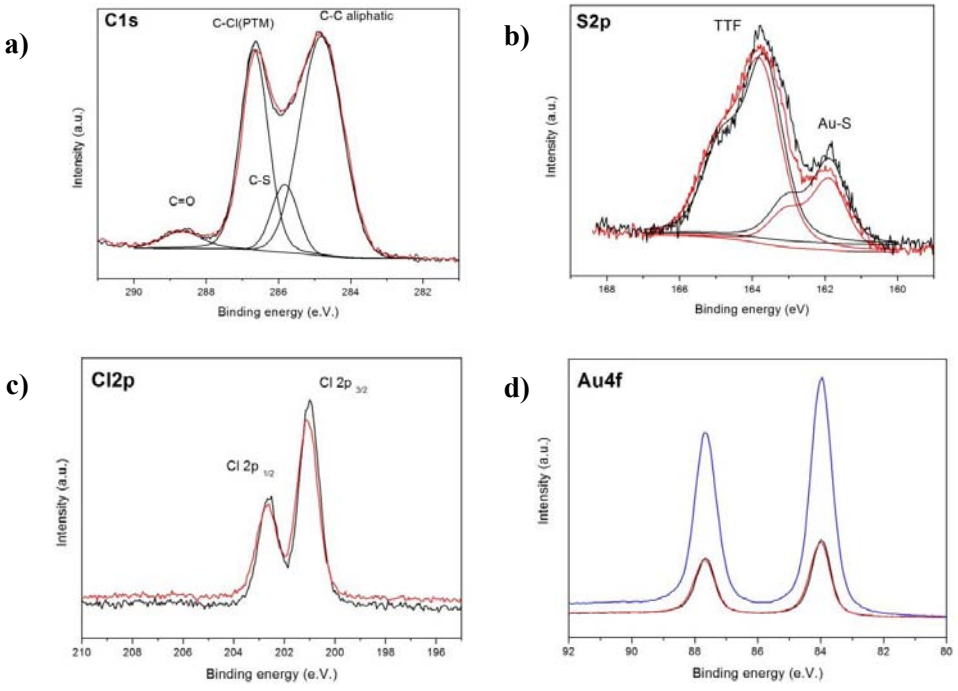

Figure S8. High resolution photoemission spectra of a) C1s b) S2p c) Cl2p and d) Au4f for SAMs of **1** (red line) and **2** (black line) measured at 500 eV. Blue line in Au4f is the blank (bare gold).

3.7. Thickness of SAMs 1 and 2

Film thickness of SAMs of **1** and **2** was estimated from the high resolution PE spectrum of Au_{4f} taken at 630 eV, shown in Figure S8d, by evaluating the attenuation of the Au $4_{f7/2}$ peak of a sputtered substrate and for each functionalized substrate according to Equation 1 where I and I_o correspond to the substrate intensity of the SAM covered and bare surface, respectively; d is the SAM thickness, and θ is the detection angle with respect to the surface normal.

$$I = I_o \exp(-d/\lambda\cos\theta) \qquad \text{(Eq. 1)}$$

In this case, θ was zero since the analyser was normal to the sample surface obtaining a deviation of the emission angle from the surface normal of 0. λ is the photoelectron attenuation length and is characteristic of each system. λ depends on the kinetic energy of the photoelectrons and for these measurements it was assumed a value of 18.2 Å as reported for adenine[S1] as model organic system, supported by the fact that similar values have been reported for organic systems. We obtained a thickness (d) of 20.92 and 20.72 Å for **SAM 1** and **SAM 2** respectively.

3.8. Surface coverage

To calculate the surface coverage of the SAMs **1** and **2**, we calculated the integrated intensity of Cl 2*p* spectra (I_{Cl}) of the SAMs (1 and 2) and $S(CH_2)_{10}CH_2Cl$ ($SC_{11}Cl$) SAMs (listed in the Table S1 below). We performed the least-square peak fit analysis with Voigt functions (Lorentzian (30%) and Gaussian (70%)) using XPSpeak software, and the sloping background was modelled using Shirley plus linear background correction.[S2,S3] Since the Cl atoms were connected to the terminal groups of the SAMs which the attenuation over distance could be rejected, the I_{Cl} can be solely related to the surface coverage of the SAMs. The relative surface coverage was calculated comparing the I_{Cl} of the SAMs **1** and **2** (divided by 14 prior; SAMs **1** and **2** contains 14 Cl atoms) against that of $SC_{11}Cl$ SAMs. The surface coverage of S $SC_{11}Cl$ SAMs on Ag surface has been reported before and is 1.1×10^{-9} mol/cm^2.[S4] Thus, we compared the values of I_{Cl} of the SAMs **1** and **2** against that of the $SC_{11}Cl$ SAMs to calculate the absolute surface coverage of the SAMs **1** and **2** (Table S1). We estimated the uncertainties are about 5% from the fitting errors of Cl 2*p* spectra. However, we have noticed the 14 Cl atoms on the PTM moiety were not all exposed at the top of the SAMs, and at least 4 Cl atoms (connected to the phenyl ring with alkyl chain) could be taken into attenuation over the half-length (~6.3 Å) of the PTM moiety. Thus, the absolute surface coverage calculated by XPS here was underestimated about at least 13% (= / - /). Nevertheless, the relative surface coverages are for all the SAMs the same which support our conclusion that we did not change the supramolecular structure of the SAMs.

Table S1. The values of I_{Cl}, relative surface coverage and absolute surface coverage.

SAMs	I_{Cl} at 90° take-off angle	Relative surface coverage[a]	Absolute surface coverage ($\times 10^{-9}$ mol/cm^2)
SAM 1	39184	0.11	0.12
SAM 2	42643	0.11	0.12
$SC_{11}Cl$	26450	1	1.10

[a] The relative surface coverage is calculated from $I_{Cl}(SC_{11}Cl)$ / (I_{Cl}(SAM **1** or **2**) / 14).

3.9. Calculation of LUMO energy levels from NEXAFS spectra

We used the binding energy of the C 1*s* core level of the PTM (Figure 6) to calculate the SUMO or LUMO level with respect to the Fermi level of the electrode from the NEXAFS spectra, with a correction of 0.5 eV for core-hole exciton binding energy to take into account the core-hole attraction effect. Others have reported correction factor in the range of 0.1 – 2.0 eV,[S5] but we have used 0.5 eV also for other types of SAMs in the supporting information of reference.[S6] We estimated the LUMO energy position (with respect to the vacuum level) from the first resonance peak of the NEXAFS spectra. In principle, the LUMO energy respected to the Fermi level is equal to the difference between the photon energy of the $4e_{1g}$ peak (PE_{LUMO}) and the C1s binding energy of cyclopentadienyl ring (BE_{Cp}). However, during the X-ray adsorption process, the electron is excited from the core level leaving behind a hole in the core level. This hole interacts with the electron in the excited state lowering the energy of the LUMO. Here we correct the estimated LUMO energy for this core-hole exciton binding energy ($BE_{exciton}$) using equation 2 and BEexciton = 500 meV taken from reference S10 which is typically used in thin organic films.

$$LUMO = PE_{LUMO} - BE_{Cp} + BE_{exciton} \quad \text{(Eq. 2)}$$

3.10. Calculation of orbital energies from CV

Information about the HOMO and LUMO energies of electroactive molecules grafted on an electrode, relative to vacuum, can be extracted from cyclic voltammograms using Equation 3; where $E_{abs,NHE}$ is the absolute potential energy of the normal hydrogen electrode (-4.5 eV), and $E_{1/2,NHE}$ is the formal half-wave potential of the grafted molecule *vs.* the normal hydrogen electrode (NHE).

$$E_{HOMO} = E_{abs,NHE} - eE_{1/2,NHE} \quad \text{(Eq.3)}$$

3.11. Fabrication of Au^{TS}-SAMs//GaO_x^{cond}/EGaIn junctions

The fabrication of the SAM-based junctions with cone-shaped tips of GaO_x^{cond}/EGaIn were reported previously.[S7] Briefly, in our experiments we grounded the bottom electrode on which a gold probe penetrating the SAMs and the top-electrode of GaO_x^{cond}/EGaIn was biased from 0V →2.0 V→ 0V →-2.0 V → 0V, with a step size of 50 mV, and a delay of 0.1 s, for the *J*(V) curve. The statistical analysis follows previous reported methods[4] and the results are listed in Table 1 in the main text.

4. References of the Supporting Information

[**S1**] Lamont, C. and Wilkes, J. (1999) reported the expression $l = 0.3E0.64$ to calculate the attenuation length of photoelectrons of n-alkanethiols monolayers on gold in the range of 300-1000 eV of KE. Using this equation a value of $l = 16.94$ Å is obtained, which is close to the value assumed.

[**S2**] Tour, J. M. *et al.* Self-assembled monolayers and multilayers of conjugated thiols, alpha,omega-dithiols, and thioacetyl-containing adsorbates - understanding attachments between potential molecular wires and gold surfaces. *J. Am. Chem. Soc.* **117**, 9529-9534 (1995).

[**S3**] Ishida, T. *et al.* High-resolution X-ray photoelectron spectra of organosulfur monolayers on Au(111): S(2p) spectral dependence on molecular species. *Langmuir* **15**, 6799-6806 (1999).

[**S4**] Wang, D. *et al.* Tuning the tunneling rate and dielectric response of sam-based junctions via a single polarizable atom. *Adv. Mat.* **27**, 6689-6695 (2015).

[**S5**] Stohr, J. *NEXAFS Spectroscopy*. Berlin. (1992).

[**S6**] Yuan, L., Breuer, R., Jiang, L., Schmittel, M. & Nijhuis, C. A. A molecular diode with a statistically robust rectification ratio of three orders of magnitude. *Nano Lett.* **15**, 5506-5512 (2015).

[**S7**] Nerngchamnong, N. *et al.* The role of van der Waals forces in the performance of molecular diodes. *Nat. Nanotechnol.* **8**, 113-118 (2013).

Chapter 6

Conclusions

In the framework of this Thesis we have prepared and studied different functional molecular materials based on donor-acceptor (D-A) dyads formed by the electron-acceptor polychlorotriphenylmethyl (PTM) radical and the electron-donor tetrathiafulvalene (TTF) linked by different conjugated bridges (Figure 6.1). These TTF-π-PTM radical systems can exhibit interesting physical properties such as NLO properties or bistability in solution, conductivity in solid state or electrical rectification on surfaces. Thus, these interesting dyads could find application in the field of molecular electronics as molecular switches, NLO-phores, conductors or rectifiers in the field of molecular electronics.

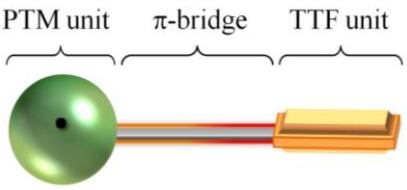

Figure 6.1. Schematic representation of a TTF-π-PTM dyad.

Specifically, we have reached the following conclusions:

1. In the first Section of Chapter 2, we have studied the temperature-induced switching of TTF-PTM radical dyad **1** in DMF solution between diamagnetic dimers $\mathbf{[1]_{2\ LT}}$, observed at room temperature, and paramagnetic monomers $\mathbf{1_{HT}}$ at high temperature (Figure 6.2). Different optical and magnetic properties were observed for the two different states of this supramolecular switch when using the temperature as external input. Such changes are due to the subtle interplay of intra- and intermolecular CT processes occurring between the subunits of the involved species.

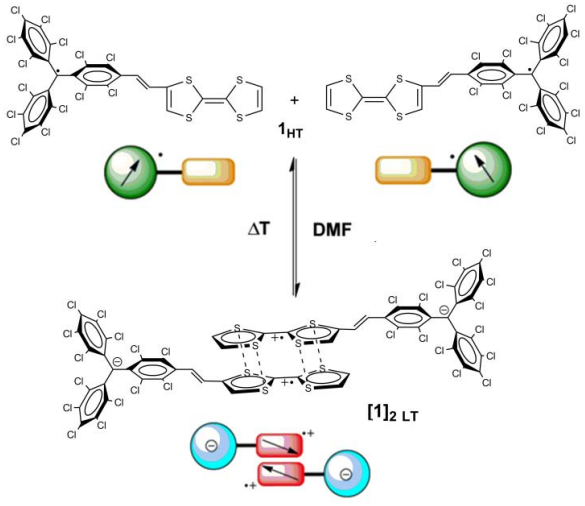

Figure 6.2. Schematic representation of the reversible temperature-induced supramolecular switching of TTF-PTM (**1**) between diamagnetic dimers at low temperature ($\mathbf{1_{LT}}$) and paramagnetic monomers at high temperature ($\mathbf{1_{HT}}$).

2. In the second Section of Chapter 2, we have synthesized the diradical A-D-A triad **2** composed by two PTM radical subunits connected through a TTF-vinylene bridge, that can reversibly modulate the optical, electronic and magnetic properties by one-electron reduction and oxidation in CH_2Cl_2 solution (Figure 6.3). Interestingly, the modification of electron delocalization and magnetic coupling was observed when the charged species were generated and the changes were rationalized by theoretical calculations.

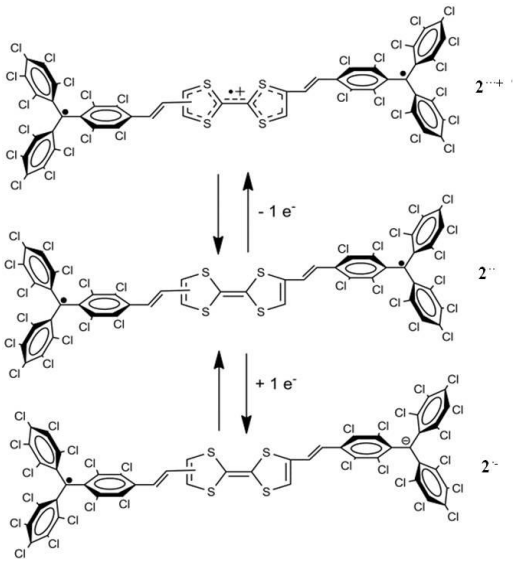

Figure 6.3. Molecular structures of diradical **2**, mixed-valence $\mathbf{2}^{\bullet -}$ and triradical cation $\mathbf{2}^{\bullet\bullet\bullet +}$.

3. In Chapter 3, we have reported the synthesis and characterization of a family of TTF-π-PTM radical derivatives (**1, 3** and **4**) increasing the number of vinylene units between the PTM and TTF units (Figure 6.4). We have studied the intramolecular charge transfer and non-linear optical (NLO) properties in solution and their dependence on the open-shell structure and on the bridge length of this family of compounds. Interestingly, an enhanced NLO response was observed when the PTM was in its radical form as well as the length of the bridge became larger.

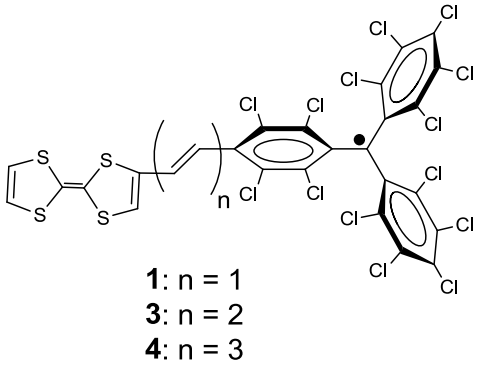

Figure 6.4. Molecular structures of radical dyads **1**, **3** and **4**.

4. In Chapter 4, we have synthesized and characterized the MPTTF-PTM radical dyad **5** that shows an interesting self-assembly architecture with segregated donor and acceptor units in the crystal structure (Figure 6.5). Moreover, we have studied the appearance of conductivity in single crystals of radical dyad **5** induced by pressure. The semiconductor behavior of **5** was mainly attributed to the enhanced electronic bandwidth *W* due to incorporation of TTF units which force the formation of close packed stacks of molecules and to the reduction of the effective Coulomb *U* interaction attributed to the enhanced electron delocalization in the system due to incorporation of a substituent donor unit.

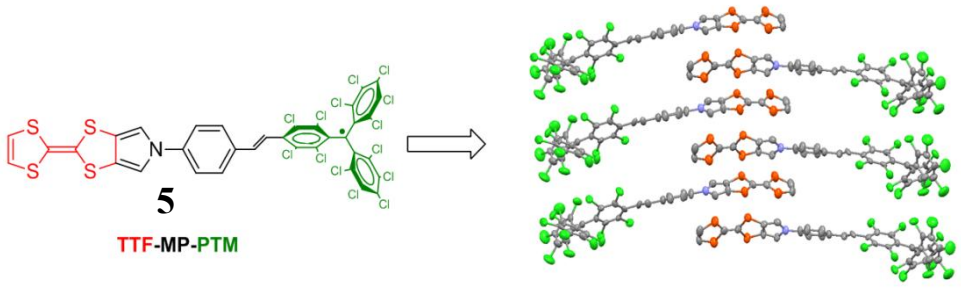

Figure 6.5. Molecular structure and crystal packing of TTF-MP-PTM radical (**5**).

5. Finally, in Chapter 5 we have synthesized and characterized the radical (**6**) and non-radical (**6-H**) dyads that were functionalized with a disulfide group in order to prepare self-assembled monolayers (SAMs) on gold (Figure 6.6). These SAMs were fully characterized and the charge transport through the SAMs was measured in order to evaluate these systems as possible molecular rectifiers. Whereas SAMs of radical dyad **6** didn't show any rectification behavior, junctions with SAMs of non-radical dyad **6-H** showed a moderate rectification ratio.

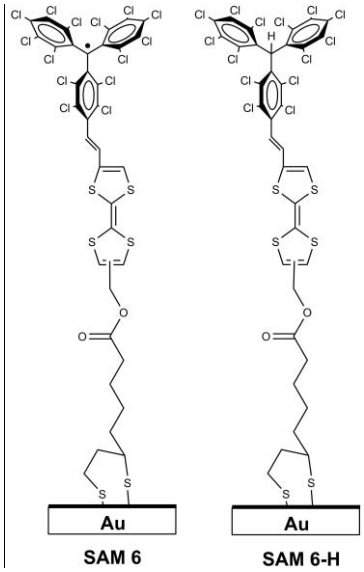

Figure 6.6. Idealized schematic representation of self-assembled monolayers formed by **6** (**SAM 6**) and **6-H** (**SAM 6-H**) on gold.

List of publications

1. Induced Self-assembly of a TTF-based Open-Shell Dyad through an Intramolecular Electron Transfer. J. Guasch, L. Grisanti, V. Lloveras, J. Vidal-Gancedo, M. Souto, D. Morales, M. Vilaseca, C. Sissa, A. Painelli, I. Ratera, C. Rovira and J. Veciana. *Angew. Chem. Int. Ed*. **2012**, *51*, 1–6.
2. Bistability of Fc-PTM-Based dyads: The role of the donor strength. J. Guasch, L. Grisanti, S. Jung, D. Morales, G. D'Avino, M. Souto, X. Fontrodona, A. Painelli, F. Renz, I. Ratera, and J. Veciana. *Chem. Mater.* **2013**, *25* (5), 808–814.
3. Intra- and Intermolecular Charge Transfer in Aggregates of Tetrathiafulvalene-Triphenylmethyl Radical Derivatives in Solution. J. Guasch, L. Grisanti, M. Souto, V. Lloveras, J. Vidal-Gancedo, I. Ratera, A. Painelli, C.Rovira, and J. Veciana. *J. Am. Chem. Soc.* **2013**, *135*, 6958−6967.
4. Thermomagnetic Molecular System Based on a TTF-PTM Radical: Switching the Spin and Charge Delocalization. M. Souto, J. Guasch, V. Lloveras, P. Mayorga, J. T. López Navarrete, J. Casado, I. Ratera, C. Rovira, A. Painelli, and J. Veciana. *J. Phys. Chem. Lett.* **2013**, *4* (16), 2721–2726.
5. Syntheses and solid state structures of cyclam-based copper and zinc compounds. L. G. Alves, M. Souto, F. Madeira, P. Adão, R. F. Munhá, A. M. Martins. *J. Organomet. Chem.* **2014**, *760*, 130-137.
6. Intramolecular electron transfer and charge delocalization in bistable donor–acceptor systems based on perchlorotriphenylmethyl radicals linked to ferrocene and tetrathiafulvalene units. M. Souto, D. Morales, J. Guasch, I. Ratera, C. Rovira, A. Painelli, and J. Veciana. *J. Phys. Org. Chem.* **2014**, *27*, 465-469.
7. Self-assembled architectures with segregated donor and acceptor units of a dyad based on a monopyrrolo-annulated TTF-PTM radical. M. Souto, M. Solano, I. Ratera, M. Jensen, D. Bendixen, F. Delchiaro, A. Girlando, A. Painelli, J. O. Jeppesen, C. Rovira and J. Veciana. *Chem. Eur. J.* **2015**, *21*, 8816-8825.
8. Three Redox States of a Diradical Acceptor-Donor-Acceptor Triad: Gating the Magnetic Coupling and the Electron Delocalization. M. Souto, V. Lloveras, S. Vela, M. Fumanal, I. Ratera, J. Veciana. *J. Phys. Chem. Lett.* **2016***, 7,* 2234-2239.
9. Pressure-Induced Conductivity in a Neutral Non-Planar Spin-Localized Radical. M. Souto, H. Cui, M. Peña-Álvarez, V. G. Baonza, H. O. Jeschke, M. Tomic, R. Valentí, D. Blasi, I. Ratera, C. Rovira, J. Veciana. *J. Am. Chem. Soc.* **2016** *Just Accepted.*

10. Non-Linear Optical Properties of Push-Pull TTF-p-PTM Radicals: The Role of the Open-Shell structure and Bridge Length. M. Souto, V. Pia, I. Ratera, E. Ortí, W. Wenseelers, J. Veciana. *In preparation.*
11. Grafting TTF-PTM dyads on Surfaces: Towards New Molecular Rectifiers and Switches. M. Souto, L. Yuan, I. Ratera, C. A. Nijhuis, J. Veciana. *In preparation.*